Navarro-Garcia Jose Alberto (Orcid ID: 0000-0002-0317-4888)

Ruiz-Hurtado Gema (Orcid ID: 0000-0003-3482-0915)

Title: Enhanced Klotho availability protects against cardiac dysfunction induced by uraemic cardiomyopathy by regulating Ca^{2+} handling

José Alberto Navarro-García[1], Angélica Rueda[2], Tatiana Romero-García[2], Jennifer Aceves-Ripoll[1], Elena Rodríguez-Sánchez[1], Laura González-Lafuente[1], Carlos Zaragoza[3], María Fernández-Velasco[4], Makoto Kuro-o[5], Luis M. Ruilope[1, 6, 7], Gema Ruiz-Hurtado[1,6]*

[1]Cardiorenal Translational Laboratory, Institute of Research i+12, Hospital Universitario 12 de Octubre, Madrid, Spain. [2]Departamento de Bioquímica, Centro de Investigación y de Estudios Avanzados del IPN, México City, D.F., México. [3]Departamento de Cardiología, Unidad de Investigación Mixta Universidad Francisco de Vitoria/Hospital Ramón y Cajal (IRYCIS)/CIBER-CV; [4]IdiPAZ Institute for Health Research/CIBER-CV, Madrid, Spain. [5]Division of Anti-ageing Medicine, Centre for Molecular Medicine, Jichi Medical University, Shimotsuke, Tochigi, Japan. [6]CIBER-CV, Hospital Universitario 12 de Octubre, Madrid, Spain. [7]School of Doctoral Studies and Research, European University of Madrid, Madrid, Spain.

*To whom correspondence should be addressed: Gema Ruiz-Hurtado, Centro de Investigación, Instituto de Investigación imas12, Hospital Universitario 12 de Octubre, Avenida de Córdoba s/n, 28041, Madrid. Phone: +34 91 3908001. Email: gemaruiz@h12o.es

Word count (excluding abstract, methods, references and figure legends): **5.127**

Running Title: Klotho protects cardiac Ca^{2+} mishandling in CKD

Acknowledgments: We thank to Dr. Monserrat Grau Sanz for her excellent assistance with experimental animal facilities, Dr. Inés García-Consuegra Galiana (from the Proteomic facility of Hospital 12 de Octubre (i+12)) for her technical assistance, Dr. Agustín Guerrero-Hernández

(Department of Biochemistry, Cinvestav-IPN) for helpful recommendations on Ca^{2+} measurement analysis, and Dr. Blanca Miranda for her continuous support.

Funding: This work was supported by several projects from the Instituto de Salud Carlos III, Ministry of Economy, Industry and Competitiveness [PI14/01841, CP15/00129, PI17/01093, PI17/01193, PI14/01078, PI17/01344, MSII16/00047], Fundación SENEFRO, Sociedad Española de Cardiología (SEC), Fundación Renal Íñigo Álvarez de Toledo (FRIAT), and cofunded by the European Regional Development Fund (Fondos FEDER), and approved by the Ethics Commitees of our Institution.

Author contributors: G.R-H and JA.N-G designed and conceptualised the experiments. JA.N-G, T.R-G, G.R-H performed the experiments. JA.N-G, A.R., T.R-G, E.R-S, L.G-L and G.R-H analysed the data. C.Z. carried out, analysed and interpreted echocardiograms. G.R-H, M.F-V, LM.R and M.K-o provided reagents and materials. JA.N-G, M.F-V, LM.R and M.K-o helped with data interpretation. JA.N-G and G.R-H wrote the manuscript.

Conflict of Interest: The authors declare no conflicts of interest.

Declaration of transparency and scientific rigour: This Declaration acknowledges that this paper adheres to the principles for transparent reporting and scientific rigour of preclinical research as stated in the *BJP* guidelines for Design & Analysis, Immunoblotting and Immunochemistry, and Animal Experimentation, and as recommended by funding agencies, publishers and other organisations engaged with supporting research.

What is already known:

- CKD patients present alterations in mineral metabolism components including a decline in klotho protein expression
- Recent studies point to klotho as a new anti-ageing factor with cardioprotective properties

What this study adds:

- Klotho deficiency alters systolic Ca^{2+} release and contractile function, and increases pro-arrhythmogenic diastolic Ca^{2+} leak
- Recombinant klotho treatment prevents cardiac Ca^{2+} mishandling and RyR hypersensitivity in CKD

Clinical significance:

Recombinant klotho is a promising new prophylactic strategy to reduce cardiac functional alterations in CKD

Summary (in 50 words)

Klotho, named after the Greek goddess Klotho who spun the thread of life, is an ageing-suppressing protein. Renal disease is a form of premature ageing with a diminution in klotho synthesis which courses with fatal cardiovascular events. We demonstrate that klotho supplementation blocks cardiac dysfunction associated with renal disease.

Abstract

Background

Klotho is a membrane-bound or soluble protein originally identified as an age-suppressing factor and regulator of mineral metabolism. Klotho deficiency is associated with the development of renal disease, but its role in cardiac function in the context of uraemic cardiomyopathy is unknown.

Experimental Approach We explored the impact of klotho on cardiac Ca^{2+} cycling. We analysed Ca^{2+} handling in adult cardiomyocytes from klotho-deficient (*kl/kl*) mice and from a murine model of 5/6 nephrectomy (Nfx). We also studied the effect of exogenous klotho supplementation, by chronic recombinant klotho treatment, or endogenous klotho overexpression, using transgenic mice overexpressing klotho (*Tg-Kl*), on uraemic cardiomyopathy. Hearts from Nfx mice were used to study Ca^{2+} sensitivity ryanodine receptor and its phosphorylation state.

Key results

Cardiomyocytes from *kl/kl* mice showed a decrease in the amplitude of intracellular Ca^{2+} transients and cellular shortening together with an increase in pro-arrhythmic Ca^{2+} events compared with cells from wild-type mice. Cardiomyocytes from Nfx mice exhibited the same impairment in Ca^{2+} cycling than *kl/kl* mice. Changes in Nfx cardiomyocytes were explained by

higher sensitivity of ryanodine receptors to Ca^{2+} and their increased phosphorylation at the calmodulin kinase type II and protein kinase A sites. Ca^{2+} mishandling in Nfx-treated mice was fully prevented by chronic recombinant klotho administration or transgenic klotho overexpression.

Conclusions and Implications

Klotho emerges as an attractive therapeutic tool to improve cardiac Ca^{2+} mishandling observed in uraemic cardiomyopathy. Strategies that improve klotho availability are good candidates to protect the heart from functional cardiac alterations in renal disease.

Key words: Klotho, uraemic cardiomyopathy, chronic kidney disease, Ca^{2+} mishandling, ryanodine receptors.

Abbreviations:

BUN: Blood Urea Nitrogen; CaMKII: Ca^{2+}/calmodulin-dependent protein kinase II; CKD: Chronic Kidney Disease; EF: Ejection fraction; FGF-23: Fibroblast Growth Factor-23; FGFR: Fibroblast Growth Factor Receptor; Hz: Hertz; Mhz: Megahertz; Nfx: 5/6 nephrectomy; PKA: Protein Kinase A; rKL: recombinant klotho; sKL: soluble klotho; SR: Sarcoplasmic Reticulum; SERCA: Sarcoplasmic Reticulum Ca^{2+}-adenosine triphosphatase 2a; RyR: Ryanodine Receptor.

Introduction

Risk of cardiovascular disease increases as renal function declines (Go, Chertow, Fan, McCulloch & Hsu, 2004; Herzog et al., 2011), and cardiovascular disease is the major cause of mortality in patients with chronic kidney disease (CKD). Among the components of bone mineral metabolism, alterations in klotho protein and fibroblast growth factor (FGF)-23 axis seem to be important contributors to the high cardiovascular risk in this patient group (Gutiérrez et al., 2008; Isakova et al., 2018; Isakova et al., 2011). FGF-23 is a circulatory hormone that mainly targets the kidney, where it controls systemic phosphate homeostasis. The phosphaturic action of FGF-23 is dependent on renal expression of membrane-bound klotho, a powerful regulator of ageing and life-span (Kuro-o et al., 1997). Klotho is predominantly synthesised in the kidney where it binds to FGF receptors (FGFRs), increasing their affinity for FGF-23 and promoting urinary phosphate excretion (Urakawa et al., 2006). Klotho expression diminishes as renal function deteriorates, and this reduction might be responsible

for the resistance to FGF-23 observed along the course of CKD (Pavik et al., 2013). Membrane-bound klotho can be shed by the action of secretases and released into circulation as a soluble form. Circulating soluble klotho (sKL) has several pleiotropic functions that are poorly understood, including an apparently cardioprotective action that is independent of FGF-23 and phosphate (Hu et al., 2017; Xie, Cha, An, Kuro-O, Birnbaumer & Huang, 2012; Xie, Yoon, An, Kuro-o & Huang, 2015). Accordingly, high soluble klotho levels are associated with a lower risk of developing cardiovascular disease and low soluble klotho levels are related to cardiac dysfunction, at least when advanced age is considered (Semba et al., 2011). Several recent clinical studies have shown that low circulating soluble klotho levels associate with elevated risk of cardiovascular mortality or hospitalisation due to cardiovascular events (including heart failure development, myocardial infarction or stroke) in patients with stable ischemic heart disease (Bergmark et al., 2019) or on hemodialysis (Memmos et al., 2019). Thus, there is a need to determine whether klotho can directly regulate cardiomyocyte function and cardiac rhythm in the setting of renal disease, and to elucidate the underlying mechanisms involved in the potential cardioprotective actions of klotho.

The increased cardiovascular morbidity and mortality linked to renal dysfunction is due, at least in part, to the high prevalence of heart failure and arrhythmias in patients with CKD mainly those undergoing dialysis (Charytan et al., 2016; Verde et al., 2016; Wanner, Amann & Shoji, 2016). Indeed, cardiovascular deaths account for ~50% of all deaths in CKD, especially in patients on dialysis, which is chiefly due to fatal arrhythmias (Coll et al., 2018). Alterations in intracellular Ca^{2+} cycling, such as changes in Ca^{2+} release from the sarcoplasmic reticulum (SR) mediated by ryanodine receptor (RyR) channels in cardiomyocytes, are well documented mechanisms involved in cardiac dysfunction and arrhythmias (Bers, 2014; Nattel, Maguy, Le Bouter & Yeh, 2007). Cardiac contraction is triggered by an action potential that induces a small Ca^{2+} influx via sarcolemmal L-type Ca^{2+} (I_{CaL}) channels, triggering a greater release of Ca^{2+} from the SR by RyR channels. This elevation in cardiomyocyte Ca^{2+} transients stimulates cardiomyocyte contraction (Bers, 2002). Relaxation is initiated when Ca^{2+} is pumped out from the cytosol by two chief mechanisms: 1) Ca^{2+} re-uptake to the SR by the Ca^{2+}-adenosine triphosphatase 2a pump SERCA (~92%), and 2) Ca^{2+} extrusion to the extracellular medium by the Na^{+}/Ca^{2+} exchanger NCX (~7%) (Bers, 2002). An increase in RyR channel sensitivity, evoking higher spontaneous diastolic SR-Ca^{2+} leak, is known to increase the risk of malignant arrhythmias (Navarro-García et al., 2019). Whether Ca^{2+} handling alterations also

occur in the context of CKD, and whether klotho could induce cardioprotection in this context by modulating intracellular Ca^{2+} handling remains unknown.

Here, we used klotho-deficient (*kl/kl*) mice to question if klotho is necessary for correct cardiomyocyte function. Furthermore, we established a murine model of CKD by 5/6 nephrectomy to test the hypothesis that strategies directed to improve klotho availability – supplied exogenously (recombinant) or endogenously enhancing its expression – could prevent cardiac dysfunction related to intracellular Ca^{2+} mishandling in uraemic cardiomyopathy.

Methods

Animals

Male C57BL/6J mice (20-23 g, 6 weeks of age; IMSR_JAX:000664) were purchased from Charles River Laboratories International Inc. (Wilmington, MA, USA; SCR_003792). Mice were bred and housed under specific pathogen-free conditions in the Experimental Animal Centre of Hospital Universitario 12 de Octubre, Madrid, Spain. All experiments were performed after approval of the Bioethical Committee *Universidad Autónoma de Madrid*; the animal protocol was approved by the General Direction of Agriculture and the Environment at the Environment Council of Madrid (PROEX 053/16) following of the guidelines for ethical NIH Guide for the Care and Use of Laboratory Animals and Guidelines for Ethical Care and Welfare (2013/175) of Experimental Animals of the European Union (2010/63/EU) and following the ARRIVE guidelines for reporting experiments involving animals (Kilkenny, Browne, Cuthill, Emerson & Altman, 2010; McGrath, Drummond, McLachlan, Kilkenny & Wainwright, 2010). Animals were maintained at controlled temperature (23-25ºC) on a 12-hours light/dark cycle with ad libitum access to water and a standard diet (ROD14, Altromin Spezialfutter GmbH & Co. KG, Lage, Germany). Animals were housed in groups of 4 per cage of 553 cm2 by 20.8 cm depth (polysulfone cage type II L, SODISPAN, Madrid, Spain) with standard wood chip (ECO-PURE 7 Chips, Tapvei®, Estonia). All efforts were made to reduce the number of animals required to obtain reliable results and minimise the suffering of the animals based on the 3Rs rule of replacement, refinement, and reduction. The viability of the ventricular cardiomyocyte isolation process was established when the percentage of relaxed and rod-shaped cardiomyocytes in total cell count was equal or bigger than 70 % (Shioya, 2007). No difference was observed in the viability of the cardiomyocyte isolation process between all experimental groups.

Experimental model of chronic kidney disease and treatments

Mice underwent *Sham* or 5/6 nephrectomy (Nfx) surgery to induce CKD. Nfx was performed in a two-step procedure under isoflurane anaesthesia (1.5% v/v, isoflurane/oxygen). In the first step an abdominal incision was made, and the upper and lower poles of the left kidney were removed, leaving an intact segment around the hilum (experimental week 0). One week later, a dorsal incision was made and the right kidney was completely removed (Gagnon & Gallimore, 1988). Sham-operated mice followed the same protocol without the removal of the kidneys. Metoxicam (0.06 mL kg^{-1}, s.c. single dose) was used as analgaesia after surgeries. After Sham or Nfx surgery mice were blindly randomized to receive either vehicle solution (0.9% sodium chloride) or murine recombinant klotho (rKL, at the dose of 0.01 mg kg^{-1} of weight per day). Mice were treated at the same hour in the morning every day for 6 weeks via intraperitoneal injection as described before (Hu et al., 2017). Macroscopic parameters were analysed in 16 *Sham*, 20 Nfx, 17 *Sham*+rKL and 22 Nfx+rKL mice. 10 mice in each group were used for biochemical parameters, 5-7 mouse hearts per group were used for ryanodine binding analysis and 5 mice per group were used for echocardiogram analysis. Cardiomyocytes obtained from 5 *Sham*, 6 Nfx, 5 *Sham*+rKL and 6 Nfx+rKL mice were used to Ca^{2+} handling analysis.

Echocardiography

Mouse hearts were visualized by echocardiography, using the Vivid Q ultrasound system (GE Healthcare), with a coupled linear sonar of 14 Mhz. A single investigator blinded to the experimental groups performed the analysis. Measurements were carried out with mice under isoflurane anaesthesia (1.5% v/v, isoflurane/oxygen) in order to keep a heart rate of about 400 beats/minute. Body hair was shaved, and parasternal images of the short axis of the heart were obtained in a bidimensional mode (B), for anatomical visualization. Taking as a reference the papillary muscles, the functional analysis of cardiac contractility was carried out by an ultrasound M mode, to determine ejection fraction (EF) using cardiac analysis software.

Klotho-hypomorphic and klotho-overexpressing mice

Transgenic (*Tg-Kl*), and klotho hypomorphic (*kl/kl)* mice were kindly provided by Dr. Kuro-o and bred in our animal facilities.

Male *kl/kl* mice (8 g of weight) and their +/+ littermates (20 g of weight) were used at 6-8 weeks of age. Macroscopic parameters were analysed in 22 +/+ and 19 *kl/kl* mice. 10 mice in

each group were used for biochemical parameter analysis, and 5 mice per group were used for Ca^{2+} handling analysis.

Tg-Kl 6-week-old mice with a weight between 20-22 g underwent *Sham* (*Sham-Tg-Kl*) or Nfx (Nfx-*Tg-Kl*) surgery as described before. Biochemical parameters were analysed in 5 *Sham-Tg-Kl* and 8 Nfx-*Tg-Kl* mice, and 5 mice per group were used for Ca^{2+} handling analysis.

Serum and urine biochemistry

Plasma levels of phosphorus (Abcam, Cambridge, UK), urea and blood urea nitrogen (BUN) (BioAssays System, Hayword, CA), and FGF-23 (Immunotopics, Inc., San Clemente, CA) were measured by ELISA following the manufacturers' instructions. Mouse soluble α-klotho assay kit (IBL International, Hamburg, Germany) was used to measure sKL in urine samples.

Cardiomyocyte isolation

Adult male mice (6–8-week-old +/+ or *kl/kl*, 14-week-old WT-*Sham*, Nfx, *Sham*+rKL or Nfx+rKL and *Tg-Kl-Sham* or *Tg-Kl*-Nfx, blindly selected) were anaesthetised with sodium pentobarbital-heparin (100 mg/kg, i.p.). Mice were sacrificed and hearts were rapidly removed and cannulated via the ascending aorta on a Langendorff perfusion system (Navarro-García et al., 2019; Ruiz-Hurtado et al., 2015). Hearts were retrograde perfused with calcium-free Tyrode's solution supplemented with 0.2 mmol L^{-1} EGTA for 3 minutes followed by Tyrode's solution containing 0.1 mmol L^{-1} $CaCl_2$, 1 mg mL^{-1} type II collagenase (Worthington, Lakewood, NY) and 1 mg mL^{-1} BSA for 3–4 minutes at room temperature. Digested hearts were filtered through a nylon mesh (250 μm) and centrifuged at 500 rpm for 3 minutes at room temperature. The pellet was re-suspended in Tyrode's solution containing 0.5 mmol L^{-1} $CaCl_2$ and centrifuged again. Finally, the pellet was resuspended in Tyrode's solution containing 1 mmol L^{-1} $CaCl_2$. Tyrode's solution contained (in mM): 130 NaCl, 5.4 KCl, 0.4 NaH_2PO_4, 0.5 MgCl2, 25 HEPES, 22 Glucose. The pH was adjusted to 7.4 with LiOH.

Confocal Ca^{2+} images analysis.

Isolated ventricular cardiomyocytes were loaded with the membrane-permeant fluorescent Ca^{2+} indicator Fluo-3 AM (5 μmol L^{-1}; Invitrogen, Carlsbad, CA) for 30 min at room temperature. Line-scan Ca^{2+} images were obtained using confocal microscopy (Meta Zeiss LSM 510, objective w.i. 40×, n.a. 1.2) at the speed of 1.5 ms/line (1000 lines per image) with a pixel size of 0.07 μm for recording Ca^{2+} transients, Ca^{2+} sparks and Ca^{2+} wave images; while for caffeine and arrhythmia protocols, confocal images were obtained at a speed of 3 ms/line (10000 lines per image) for a total duration of 30 s. All Ca^{2+} images were corrected for the

background fluorescence. In a set of experiments, Fluo-3 loaded cells were placed in a field stimulation chamber with two parallel platinum electrodes and filled with Tyrode solution. Cells were allowed to settle at the bottom of the chamber and paced at 2 Hz with a pulse generator (CS-420, Cibertec) during 1-2 min to allow steady-state intracellular Ca^{2+} transients. Then, a line was selected always in parallel to the longitudinal cell axis to be able to measure the associated cell shortening; and Ca^{2+} imaging recordings were manually initiated with the time-lapse plug-in included in Zen 2009 Imaging Software (12.09, ZEISS).

The amplitude of Ca^{2+} transients was calculated by averaging the fluorescence values in a 1.4 µm frame over time. The amplitude of Ca^{2+} transients was estimated as F/F_0, where F was the maximum value of fluorescence signal during electrical stimulation, and F_0 was the basal fluorescence at rest at each position determined as the average of the 50 lowest values on the fluorescence transient. Moreover, $\Delta F/F_0$ was calculated using the following formula: $\Delta F/F_0=(F-F_0)/F_0$. SERCA function was indirectly estimated by the decay time constant of intracellular Ca^{2+} transients, termed *Tau*, which was obtained by fitting the descending phase of the fluorescence trace to a single exponential. *K* SERCA refers to the SR-dependent fraction of the rate constant of decay of the systolic Ca^{2+} transient and was measured by subtracting the rate constant of decay of the caffeine-evoked transients from that of the systolic Ca^{2+} transients (Bode, Briston, Overend, O'Neill, Trafford & Eisner, 2011). Cell shortening was measured as the difference of cardiomyocytes length between electrical stimulation and resting. Cell shortening was expressed as the percentage of cell's shortening length. Cell shortening profiles were obtained offline by measuring the cell length from each line of Ca^{2+} transient images. SR Ca^{2+} load was estimated by perfusing cardiomyocytes with 10 mmol L^{-1} caffeine immediately after field-stimulation. Caffeine depletes the SR of Ca^{2+} stores. Caffeine-evoked Ca^{2+} transients' amplitude was measured as peak F/F_0 and was used to rate the global SR Ca^{2+} load.

In a set of experiments, spontaneous Ca^{2+} sparks were recorded in quiescent Fluo-3-loaded cardiomyocytes when electrical stimulation was stopped. Ca^{2+} sparks were considered as brief, located and rapid increments in Ca^{2+} fluorescence. Ca^{2+} sparks regions are determined as the sites where fluorescence signal increased at least 4-folds the standard deviation of the image fluorescence. This inclusion criteria limited the false events while detecting most sparks (Cheng et al., 1999). Spontaneous Ca^{2+} transients and Ca^{2+} waves in quiescent cardiomyocytes were detected as substantial spontaneous Ca^{2+} synchronic or non-synchronic release, respectively. The arrhythmic activity was measured as abnormal spontaneous Ca^{2+} transients

with automatic contractions in cardiomyocytes during a specific protocol, consisting of three cycles of 7 electric pulses followed by a recovery period.

All Ca^{2+} images were processed and analysed offline using IDL (RSI) software and homemade routines.

Ryanodine binding analysis

[^{3}H]ryanodine binding experiments were performed with left ventricle homogenates from individual hearts as described (de Alba-Aguayo et al., 2017). Specific binding was defined as the difference between the binding in the absence (total binding) and presence (non-specific binding) of 20 µM unlabelled ryanodine. The incubation medium contained (in mM): KCl 200, HEPES 20, EGTA-K salt 1, pH 7.2 with KOH. $CaCl_2$ was added as necessary to establish free Ca^{2+} at 100 nM (equivalent to diastolic Ca^{2+} concentration) and 10 µM (equivalent to systolic Ca^{2+} concentration). Ca^{2+}-EGTA ratios were calculated using the WEBMAXCLITE program v1.15 (https://web.stanford.edu/~cpatton/webmaxc/webmaxclite115.htm). Data analysis was performed using Origin (v8.1; OriginLab Corporation, Northampton, MA, USA).

Western blotting

Immunoblotting analysis complies with the recommendations on immunoblotting and immunohistochemistry in pharmacology (Alexander et al., 2018). Hearts were homogenised in 400 µL of homogenisation buffer (0.05 M Tris, 0.32 M sucrose, 0.5% CHAPS, 0.5 µM okadaic acid, and the protease inhibitors 0.1 mM PMSF, 12 µM leupeptin, 0.2 µM aprotinin and 0.5 mM benzamidine), and the pH was adjusted to 7.0. Homogenates were centrifuged at 4500 rpm for 10 minutes at 4ºC. Supernatants were collected in microtubes and 20 µg of total protein was used for western blotting. Samples were resuspended in SDS-PAGE loading buffer (4× Laemmli Sample Buffer; Bio-Rad, Hercules, CA, USA) with 10% β-mercaptoethanol, and were heated for 5 minutes at 90ºC. Samples were loaded on 4–20% SDS-PAGE gradient gels (Criterion™ TGX™ Precast Gels, Bio-Rad). Proteins were electrophoretically transferred onto PVDF membranes (Trans-Blot® Turbo™ Midi Format, 0.2 µm PVDF, Bio-Rad) on a semi-dry transfer system (Trans-Blot SD, Bio-Rad) at 2.5 A, 25 V for 10 minutes. Membranes were blocked with 5% BSA, TBS-T_{20} buffer (50 mM Tris-HCl, 150 mM NaCl and 0.1% Tween-20). Fresh antibodies solutions were used for immunoblotting. Antibodies used were as follows: Rabbit polyclonal IgG anti-phosphoRyR Ser^{2814} (AB_2617055) at 1:2000 dilution and rabbit polyclonal IgG anti-phosphoRyR Ser^{2030} at 1:2000 dilution (A010-31 and A010-32,

respectively, both from Badrilla, Leeds, UK), mouse monoclonal IgG1 anti-RyR (AB_2183054) at 1:2500 dilution and mouse monoclonal IgG1 anti-GAPDH (AB_2536381) at 1:400,000 dilution (MA3-916 and AM4300, respectively, both from Thermo Fisher Scientific, Waltham, MA, USA). HRP-conjugated secondary antibodies used were: anti-mouse IgG kappa (AB_2687626) at 1:5000 dilution and mouse anti-rabbit (AB_628497) at 1:5000 dilution (sc-516102 and sc-2357, respectively, both from Santa Cruz Biotechnology, Dallas, TX, USA).

RNA isolation and Quantitative Real-Time PCR

Total RNA was isolated from mouse hearts using the RNeasy Mini Kit (Qiagen, Hilden, Germany). Quality and quantity of RNA were assessed with NanoDrop One Microvolume UV-Vis Spectrophotometer (Thermo Fischer Scientific, Waltham, MA) and 2 µg of RNA was reverse-transcribed to cDNA using High-Capacity cDNA Reverse Transcription Kit (Applied Biosystems, Foster City, CA). Quantitative RT-PCR was performed using FastStart Essential DNA Green Master (Roche, Basel, Switzerland) in 10 µl total reaction volume on a LightCycler® 480 II (Roche, Basel, Switzerland) at optimized thermocycling settings. Relative gene expression was normalized to the ribosomal housekeeping gene 36b4 (RPLP0) and evaluated using the $2^{-\Delta\Delta Ct}$ method. The primer sequences (5´-3´) for SERCA2a (*Atp2a2*), 36b4, collagen I (*col1a1*), collagen III (*col3a1*) and atrial natriuretic peptide (*Nppa*) were as follows: *Atp2a2-Forward* TAAATGCCCGCTGTTTTGCT; *Atp2a2-Reverse* TTGTCATCTGCCAGGACCAT; *36b4-Forward* AGATGCAGCAGATCCGCAT; *36b4-Reverse* GTTCTTGCCCATCAGCACC; *col1a1-Forward* AATGGCACGGCTGTCTGCGA; *col1a1-Reverse* AGCACTCGCCCTCCCGTCTT; *col3a1-Forward* CTGTAACATGGAAACTGGGGAAA; *col3a1-Reverse* CCATAGCTGAACTGAAAACCACC; *Nppa-Forward* CTGGGACCCCTCCGATAGAT; *Nppa-Reverse* CACTCTGGGCTCCAATCCTG.

Drugs and reagents

EGTA, sodium chloride, potassium chloride, monosodium phosphate, magnesium chloride, HEPES, glucose, lithium hydroxide, potassium hydroxide, leupeptin, aprotinin, benzamidine, β-mercaptoethanol, Tween 20 and caffeine have been purchased from Sigma-Aldrich (Milan, Italy). Isoflurane has been purchased from Abbie Spain (Madrid, Spain). CHAPS has been purchased from GE Healthcare (Chicago, IL, USA). Okadaic acid-K salt has been purchased from Santa Cruz Biotechnology (Dallas, TX, USA). 4x-Laemli Sample Buffer and TBS have

been purchased from Bio-Rad (Hercules, CA, USA). Pentobarbital has been purchased from Vetoquinol (Madrid, Spain). Heparin has been purchased from ROVI (Madrid, Spain). All the reagents have been dissolved in dH2O when it was necessary.

Statistics

Group size estimation was designed to be equal considering 90% power. Inferential statistics were used to summarise the data from ≥5 animals per group. Any inequalities between experimental groups were exclusively due to the assumed animal losses related to the specific surgery (5/6 nephrectomy) used in the study. The number of animals used in this study was based on power calculation and was a total of 122. The mouse was considered as the experimental unit for echocardiography, western blotting, and ryanodine binding analyses and the whole heart was used for measurement and referred as "N". For all Ca^{2+} handling studies, the cardiomyocyte was considered as the experimental unit and referred as "n" after assessing the absence of false-positives and independence of the obtained data and the absence of clustering estimated by the intra-cluster correlation coefficient (ICC) tests for all cellular data sets and experimental models used. For Ca^{2+} handling studies, both cell number (n) and animal number (N) are shown and cardiomyocytes were isolated from at least 5 mice in each experiment. Data are presented as mean ± SEM. The data and statistical analysis comply with the recommendations on experimental design and analysis in pharmacology (Curtis et al., 2015). The data that support the results obtained in this study are available upon reasonable request from the corresponding author. Statistical significance was evaluated using paired Student's test, $\chi 2$ test or ANOVA with Newman-Keuls multiple comparison tests when appropriate (only with homogeneity and if F was significant). The Kolmogorov-Smirnov test was used to determine the Gaussian distribution of the values. All *p*-values are two-tailed and *p*-values <0.05 were considered statistically significant. All analyses were performed using GraphPad Prism v6.0 (GraphPad software Inc., San Diego, CA; SCR_002798) or Origin Pro v9.0 (OriginLab Corp., Northampton, MA; SCR_014212).

Results

Klotho deficiency alters intracellular Ca^{2+} handling and cardiomyocyte shortening, and increases pro-arrhythmogenic Ca^{2+} events

To examine whether klotho is needed for a correct cardiac function related to cardiomyocyte Ca^{2+} handling, we used an experimental model of uraemia characterised by deficiency in klotho, the klotho-hypomorphic (*kl/kl*) mouse. Macroscopic analysis showed that *kl/kl* mice were significantly smaller than their littermates +/+ (Figure 1A, Table 1). Similarly, heart and kidney weights were significantly lower in *kl/kl* mice than in +/+ mice (Table 1). Heart weight to body weight ratio (HW/BW) was significantly higher in *kl/kl* mice than in +/+ mice (Table 1). However, this increase in HW/BW ratio was not accompanied by signs of cellular hypertrophy in *kl/kl* mice, since cardiomyocyte area was significantly smaller in *kl/kl* mice than in +/+ mice (1471 ± 39.7 vs. 2428 ± 67.7 μm^2, $P<0.05$). We also measured mRNA expression levels of the atrial natriuretic peptide (ANP, *Nppa*) by quantitative RT-PCR in hearts from *kl/kl* and +/+ mice as a classic marker of cellular hypertrophy, finding *Nppa* gene expression not different between groups (1.037 ± 0.13 for +/+ vs. 0.974 ± 0.07 for *kl/kl*, arbitrary units, $P=0.674$). Moreover, to assess whether the absence of klotho expression could be accompanied by myocardial fibrosis development, collagen I and III levels were also analysed through *col1a1* or *col3a1* gene expression levels. *Kl/kl* mice showed reduced levels of collagen I and III than +/+ mice (1.008 ± 0.06 vs. 0.267 ± 0.03 arbitrary units, $P<0.05$ for *col1a1*; 1.162 ± 0.03 vs. 1.014 ± 0.08, $P<0.05$ for col3a1). Therefore, the increment in HW/BW ratio in *kl/kl* mice was not due to cardiomyocyte hypertrophy or cardiac fibrosis development. On the other hand, as expected, kidney function was impaired in *kl/kl* mice, as reflected by the significant increase in the levels of urea, BUN and FGF-23 relative to +/+ littermates (Table 1). However, no differences in phosphates serum levels were observed between both groups (Table 1), possibly as consequence of the phosphaturic action induced by the very high FGF-23 levels. We next analysed intracellular Ca^{2+} handling in cardiomyocytes isolated from both experimental groups. We studied systolic Ca^{2+} release through electrically-evoked intracellular Ca^{2+}transients. Figure 1B shows representative line-scan Ca^{2+} images (bottom panels) and fluorescence profiles (upper panels) obtained during electric field stimulation at 2 Hz, corresponding to +/+ (left panel) and *kl/kl* (right panel) cardiomyocytes. Similar differences in the amplitude of Ca^{2+} transients (F/F_0) were found between +/+ vs. *kl/kl* mice analysed by cells or by hearts (3.46 ± 0.11 vs. 1.84 ± 0.05 or 3.46 ± 0.18 vs. 1.84 ± 0.08, respectively). Intracellular Ca^{2+} transients amplitude (F/F_0) was significantly lower in *kl/kl* cells than in +/+ cells (Figure 1C). In addition, cardiomyocytes from *kl/kl* mice showed a decrease in $\Delta F/F_0$, indicating a significant decrease in the global intracellular Ca^{2+} transient in kl/kl cells (Supplemental Figure S1). The time constant of Ca^{2+} transients decay, *Tau*, was significantly longer in *kl/kl* cells than in +/+ cells (Figure 1D). This is also illustrated in the representative

fluorescence profiles normalised by the peak of Ca^{2+} transients from +/+ and *kl/kl* cells (Supplemental Figure S2), indicating that the SERCA pump was working slower in *kl/kl* cardiomyocytes. Because this slower time decay of Ca^{2+} transients could indicate a worse SR-Ca^{2+} reuptake by SERCA, we analysed the cardiac mRNA levels of SERCA2 in hearts from +/+ and kl/kl mice. As shown in Supplemental Figure S3, SERCA2 expression was significantly reduced in the hearts of kl/kl mice compared to +/+ mice. Moreover, *K* SERCA, the SR-dependent contribution of the rate constant of decay of the systolic Ca^{2+} transient, was also determined by subtracting the rate constant of decay of the caffeine-evoked transients from that of the systolic Ca^{2+} transients. *K* SERCA was significantly lower in *kl/kl* mice than in +/+ mice (Supplemental Figure S4), supporting a diminished SERCA-mediated Ca^{2+} reuptake. We next addressed whether the decrease in systolic Ca^{2+} release impaired contractile function. Representative cell shortening profiles of cardiomyocytes are shown in Figure 1E. Cell shortening was significantly lower in *kl/kl* cells than in +/+ cells (Figure 1F). Changes in systolic Ca^{2+} release can be related to alterations in SR-Ca^{2+} load. To study this, we applied caffeine to isolated Fluo-3-loaded cardiomyocytes to empty the SR of Ca^{2+}. Representative line-scan images of caffeine-evoked Ca^{2+} transients are shown in Figure 2A. Results showed that the amplitude (F/F_0) of caffeine-evoked Ca^{2+} transients was significantly lower in *kl/kl* cardiomyocytes than in cells from their littermates (Figure 2B). Caffeine-evoked Ca^{2+} transient decay was not different in cardiomyocytes from *kl/kl* mice respect +/+ mice, suggesting no alterations in Ca^{2+} extrusion through the NCX (Supplemental Figure S5).

We next analysed whether the change in SR-Ca^{2+} load was related to alterations in diastolic Ca^{2+} leak. Representative line-scan images of Ca^{2+} sparks recordings are shown in Figure 2C. We observed a significantly higher frequency of Ca^{2+} sparks in *kl/kl* cardiomyocytes than in +/+ cells (Figure 2D). Spontaneous calcium release (SCR) was also studied during diastolic recordings; spontaneous intracellular Ca^{2+} transients and Ca^{2+} waves were considered forms of SCR (Figure 2E, left and right panel, respectively). *kl/kl* cardiomyocytes had a significantly higher prevalence of SCR than +/+ cells (Figure 2F). Finally, we measured pro-arrhythmogenic Ca^{2+} events in cardiomyocytes isolated from both groups of mice. Figure 2G shows representative line-scan images of the pacing protocol. Pro-arrhythmogenic Ca^{2+} release was significantly higher in *kl/kl* cardiomyocytes than in +/+ cells (Figure 2H).

Chronic recombinant klotho administration prevents the cardiac dysfunction and impaired systolic Ca^{2+} release induced by experimental chronic kidney disease

We next employed a classical model of CKD (5/6 nephrectomy) to conduct a detailed analysis of the functional cardiac consequences in a uraemic context. Moreover, based on previous evidence demonstrating the cardioprotective action of exogenous klotho supplementation (Hu et al., 2017; Nowak et al., 2014) and after confirming that Nfx mice have significantly decreased klotho levels compared with *Sham* mice (Supplemental Figure S6) we analysed the effect of recombinant klotho (rKL) administration on cardiac function and Ca^{2+} cycling. The experimental design is shown in Figure 3A. Macroscopic analysis revealed that Nfx induced overall body weight loss independently of subsequent treatment (Table 2). Kidney weight was also significantly lower in Nfx mice than in *Sham* mice, both in vehicle- and rKL-treated mice. No differences were observed in heart weight or HW/BW ratio among groups (Table 2). No evidence of cellular hypertrophy was observed in CKD mice as demonstrated by similar cardiomyocyte area (3192 ± 93.2 vs. 3187 ± 92.7; P=0.969) and ANP expression levels (1.170 ± 0.51 vs. 0.300 ± 0.05; P=0.175) between Sham and Nfx mice. To assess whether uremic cardiomyopathy induces myocardial fibrosis development, collagen I and III levels were analysed through *col1a1* or *col3a1* expression levels by quantitative PCR in hearts from *Sham* and Nfx mice. No differences were detected between *Sham* and Nfx mice (1.031 ± 0.13 vs. 1.136 ± 0.11 arbitrary units, P=0.577 for *col1a1*; 1.058 ± 0.18 vs. 1.29 ± 0.11, P=0.338 for *col3a1*). Therefore, no signal of cardiac hypertrophy or fibrosis was detected in Nfx mice. Kidney function was impaired in Nfx mice, as demonstrated by significantly higher levels of plasma urea and BUN in the mice that underwent Nfx versus *Sham* mice (Table 2). These parameters remained elevated in rKL-treated Nfx mice, indicating that chronic rKL treatment does not recover renal function. FGF-23 levels were significantly elevated in Nfx mice, and also in Nfx animals chronically treated with rKL. By contrast, phosphorus levels were similar in all groups, likely due to the compensatory and rapid phosphaturic action evoked by the high FGF-23 levels. EF was measured by echocardiography as indicator of *in vivo* left ventricle global systolic function. EF was significantly reduced in Nfx compared with *Sham* mice, whereas Nfx treated with rKL for 6 weeks exhibited significantly improved EF than Nfx treated with vehicle, being not different than *Sham*+rKL mice (Figure 3B). Electrically-evoked Ca^{2+} transients of cardiomyocytes were studied under field stimulation of 2 Hz. Regarding contractile function, representative cell shortening profiles are shown for all groups in Figure 3C, and we observed a significant decrease in cardiomyocyte shortening in Nfx compared with *Sham* cells (Figure 3D). Whereas no effect of rKL was found in *Sham* cells for shortening, Nfx+rKL cells showed a significant increase in cell contraction compared with vehicle-treated Nfx cardiomyocytes (Figure 3C, D). Figure 3E shows representative line-scan images (bottom

panels) and fluorescence profiles (upper panels) corresponding to intracellular Ca^{2+} transients in all experimental groups. Similar differences in the amplitude of Ca^{2+} transients (F/F_0) were found between Sham and Nfx mice analysed by cells or by hearts (3.04 ± 0.12 vs. 2.11 ± 0.06 or 3.18 ± 0.32, 2.12 ± 0.14, respectively). Ca^{2+} transients amplitude (F/F_0) was significantly lower in Nfx cells than in *Sham* cells and was significantly higher in rKL-treated Nfx cells than in vehicle-treated Nfx cells (Figure 3F). Moreover, longer *Tau* values observed in Nfx cells (Figure 3G) indicate an impairment in SERCA function, which was also evident in the fluorescence profiles normalised to the peak of Ca^{2+} transients obtained from *Sham* versus Nfx cells (Supplemental Figure S7). Similarly, *K* SERCA was significantly lower in Nfx mice than in *Sham* mice (Supplemental Figure S8). rKL treatment prevented the increase in *Tau* (Figure 3G). No differences were found for *Tau* in *Sham*+rKL and Nfx+rKL cardiomyocytes (Figure 3G). Thus, chronic rKL treatment prevents the cardiac dysfunction and impairment in cell shortening observed in Nfx cardiomyocytes.

Increased diastolic Ca^{2+} leak induced by experimental chronic kidney disease is prevented by recombinant klotho administration

We evaluated SR-Ca^{2+} load in experimental CKD and the effect of rKL treatment. Figure 4A shows representative line-scan images of caffeine-induced Ca^{2+} release in each experimental group. CKD development led to a significant decrease in caffeine-evoked Ca^{2+} transient amplitude (F/F_0) (Figure 4B) and this was partially prevented in rKL-treated Nfx mice (Figure 4B). We tested whether the diastolic Ca^{2+} leak could be involved in the decreased SR-Ca^{2+} content evident in CKD. We next analysed the diastolic Ca^{2+} leak by measuring Ca^{2+} spark frequency and SCR. Figure 4C shows line-scan examples of Ca^{2+} spark recordings in the different groups of cardiomyocytes. Ca^{2+} spark frequency was significantly higher in Nfx cardiomyocytes than in *Sham* cardiomyocytes (Figure 4D). This increase was not observed in cardiomyocytes from Nfx mice treated with rKL (Figure 4D). We also analysed diastolic SCR in the form of Ca^{2+} waves (Figure 4E, left panel) and spontaneous Ca^{2+} transients (Figure 4E, right panel). The occurrence of SCR was 1.8-fold higher in Nfx cardiomyocytes (as Ca^{2+} spark frequency shown in Figure 4D) than in *Sham* cardiomyocytes (Figure 4F). However, chronic rKL treatment in Nfx mice prevented the increase of cardiomyocytes with SCR: 4% in rKL-treated Nfx mice versus 20% in vehicle-treated Nfx mice (Figure 4F), which was even lower than that from *Sham* or rKL-treated *Sham* mice (12%, Figure 4F).

Chronic recombinant klotho treatment prevents pro-arrhythmogenic Ca^{2+} events, RyR hyperactivity and phosphorylation promoted by experimental chronic kidney disease

We examined for the presence of arrhythmic behaviour dependent on Ca^{2+} cycling alterations during electrical pacing in the experimental CKD model. Figure 5A shows representative line-scan Ca^{2+} images of ventricular cardiomyocytes from *Sham* or Nfx mice treated or not with rKL and exposed to trains of electrical stimulation. When compared with *Sham*, Nfx cardiomyocytes presented a significant increase of automatic Ca^{2+} transients triggering automatic contractions between electrical pulses and after electrical pacing, and this was prevented by rKL treatment (Figure 5B). Given these findings, we next assessed whether alterations in RyR sensitivity could explain the arrhythmic behaviour in experimental CKD. Considering that ryanodine binds only to open RyRs, we determined the levels of functionally-active RyRs in equivalent systolic and diastolic Ca^{2+} conditions *in vitro*. During the systolic Ca^{2+} recordings, we found a significant 2.9-fold increase in [^{3}H]-ryanodine binding in Nfx hearts (Figure 6A) and this activity was effectively decreased by rKL, although it did not reach the levels in *Sham* animals, suggesting that additional mechanisms (i.e., SR-Ca^{2+} load) participate in decreasing the activity of RyRs. During diastolic Ca^{2+} recordings, Nfx hearts showed a significant 3.2-fold increase in the binding of [^{3}H]-ryanodine at 100 nM free [Ca^{2+}] (Figure 6B) and again rKL treatment reduced the Ca^{2+} sensitivity of RyRs in Nfx hearts (Figure 6B). As Nfx did not alter total RyR protein expression levels (Figure 6C and D upper panels), the results indicate that RyRs from Nfx hearts are more sensitive to Ca^{2+}. To determine the mechanism involved in RyR hyperactivity, we examined the phosphorylation status of cardiac RyR at two serine residues: Ser^{2030}, key phosphorylation site of protein kinase A (PKA), and Ser^{2814}, the specific phosphorylation site for Ca^{2+}/calmodulin-dependent protein kinase II (CaMKII). RyR phosphorylation at Ser^{2030} and Ser^{2814} was significantly higher in extracts from Nfx mice than from *Sham* mice (Figure 6C and D). This increased phosphorylation for Ser^{2030} and Ser^{2814} was not observed in Nfx mice treated with rKL, where basal levels of phosphorylation were similar to those of *Sham* mice.

Klotho overexpression protects against cardiomyocyte contractile dysfunction and pro-arrhythmic Ca^{2+} events in chronic kidney disease but does not eliminate renal damage

We used *Tg-Kl* mice to examine the cardioprotective role of endogenous klotho overexpression in a uraemic context. Serum levels of BUN were significantly higher in *Tg-Kl* mice subjected to Nfx than *Sham-Tg-Kl mice* (Figure 7A). No differences were observed in serum phosphorous

levels between both groups (Figure 7B), but serum FGF-23 levels were significantly higher in Nfx-*Tg-Kl* mice than in *Sham-Tg-Kl* mice (Figure 7C). Analysis of Ca^{2+} cycling in isolated cardiomyocytes from both groups revealed no differences in Ca^{2+} spark frequency (Figure 7D), SCR (Figure 7E), SR Ca^{2+} load (Figure 7F), intracellular Ca^{2+} transients (Figure 7G) or cell shortening (Figure 7H) between them. Overall, these results show that endogenous klotho overexpression protects against Ca^{2+} cycling alteration preventing contractile dysfunction and diastolic pro-arrhythmogenic Ca^{2+} release in Nfx mice.

Discussion

Klotho was initially discovered as an aging-suppressing gene in mice that extends lifespan when overexpressed (Kuro-o et al., 1997). Klotho is expressed mainly in the kidney and is composed of a very short intracellular domain, a transmembrane domain and a large extracellular domain that is susceptible to ectodomain shedding, resulting in two forms, membrane and secreted or sKL (Kuro-o, 2011). In the kidney, membrane klotho acts as a co-receptor for FGF-23, increasing the affinity of FGFRs for FGF-23-mediated phosphaturic action (Urakawa et al., 2006). sKL is a humoral factor with pleiotropic functions, including a cardioprotective action through the regulation of ion channels (Xie, Cha, An, Kuro-O, Birnbaumer & Huang, 2012) that is independent of FGF-23 and phosphate (Xie, Yoon, An, Kuro-o & Huang, 2015). CKD is considered a klotho-deficient state (Asai et al., 2012; Kuro-O, 2011). CKD courses with premature aging and is considered a global health concern due to the high prevalence, around 10% in the general population (Coresh et al., 2007). At experimental level, it has been described that models of premature aging, as klotho hypomorphic mice, develop early-stage CKD. In addition, other authors have recently described that uremic environment increases with aging in the experimental CKD model (Heveran et al., 2019). However, no studies have described overlapping effects of CKD and aging on cardiac function. Cardiac dysfunction and fatal arrhythmias, in many cases asymptomatic ventricular arrhythmias, are the leading causes of mortality in patients with CKD, especially in those with end-stage renal disease (Banerjee, 2016; Verde et al., 2016). However, the underlying mechanisms involved in this cardiorenal interaction remain enigmatic and clinicians remain uncertain about how to reduce the burden of cardiovascular events in CKD.

Our study provides the first demonstration, to our knowledge, that experimental uraemia induced by klotho deficiency or nephrectomy with reduced klotho levels is linked to a strong defect in Ca^{2+} handling, characterised by decreased systolic Ca^{2+} release and contractile

dysfunction and increased diastolic pro-arrhythmogenic Ca^{2+} release and leak accompanied by RyR hyperactivity. Our data also support the concept that preserving klotho availability, exogenously using prophylactic rKL chronic treatment or endogenously by enhancing klotho expression, could be a potential therapeutic strategy to protect the heart from the uraemic environment, including alterations in intracellular Ca^{2+} cycling that trigger contractile dysfunction and pro-arrhythmic mechanisms such as the hyperactivation of RyRs observed in CKD (Graphical Abstract). Our results show an increase in RyR activity in Nfx mice with higher spontaneous diastolic Ca^{2+} release and a diminution in SR-Ca^{2+} load. Both mechanisms are known to be associated with cardiac dysfunction and the predisposition to arrhythmias. The decrease in systolic Ca^{2+} release accompanied by a worsened contractile response, concomitant with extra-contractions and Ca^{2+} leak in the form of Ca^{2+} sparks and waves during diastole, were pro-arrhythmic Ca^{2+} events in cardiomyocytes from *kl/kl* and CKD mice. Furthermore, we identified a CKD-related increase in RyR phosphorylation as an underlying molecular explanation for the high RyR activity. Accordingly, RyR was robustly phosphorylated at its PKA (3-fold higher) and CaMKII (5-fold higher) sites in CKD mice. Similar results of PKA- and CaMKII-mediated RyR phosphorylation and its relationship with the predisposition to trigger fatal ventricular arrhythmias have also been found in experimental models of heart failure (Grimm et al., 2015; Xiao et al., 2005). This post-translational RyR modification of increased phosphorylation can be explained by the higher Ca^{2+} sensitivity of RyR at systolic and diastolic Ca^{2+} concentrations in CKD mice, which was prevented by rKL administration. Dhindwal *et al.* proposed that phosphorylation induces RyR to adopt a protein conformation that requires less energy for the transition to the open state (Dhindwal et al., 2017). Therefore, a more flexible RyR conformation might exist when the phosphorylation state is significantly increased as in CKD mice in both phosphorylation sites (Ser^{2030} and Ser^{2814}). Moreover, a similar increase in Ca^{2+} sensitivity has been observed in ventricular arrhythmia in experimental catecholaminergic polymorphic ventricular tachycardia (Fernández-Velasco et al., 2009). Gender-related differential activation of PKA and CaMKII pathways exists in rodent hearts also under pathological conditions (Bell et al., 2015; Parks, Ray, Bienvenu, Rose & Howlett, 2014). For example, in diabetic cardiomyopathy the contribution of PKA- and CaMKII-dependent pathways are less relevant in females than in male mice with a significant diminution of PKA- and CaMKII-induced RyR phosphorylation sites correlating with decreased spark-mediated calcium leak in female mice (Delgado, Gomez, Samia El Hayek, Ruiz-Hurtado & Pereira, 2019; Pereira, Ruiz-Hurtado, Rueda, Mercadier, Benitah & Gómez, 2014). Thus, it would be very likely that these pathways could be also less active in female than in male mice

in the setting of uremic cardiomyopathy. However, in our study female mice were not contemplated to avoid the potential cardioprotective effects mediated by oestrogens which could be overlapping the klotho-mediated cardioprotective actions in experimental conditions of CKD. Future experimental studies are needed to corroborate the oestrogens contribution to the Ca^{2+} mishandling observed under uremic cardiomyopathy conditions.

This study has several potential clinical and therapeutic applications for renal patients. First, our results show that decreased klotho availability, together with the presence of pathologically-elevated FGF-23 levels, might be a warning sign for increased risk of developing arrhythmic events in patients with CKD. Supporting this idea, several studies have previously shown that FGF-23 exposure alters cardiac contractility and Ca^{2+} handling in isolated adult ventricular cardiomyocytes (Navarro-García et al., 2019; Touchberry et al., 2013) and in HL-1 atrial cells (Kao et al., 2014). These findings support the notion that systemic elevation of FGF-23 likely has deleterious and direct effects on heart function in the complex pathological setting of uraemic cardiomyopathy (Faul, 2018). However, in the clinical setting further studies are still needed to decode whether FGF-23 itself is an independent uremic factor able to play a relevant role in the cardiac events accompanying the decline of renal function. Accordingly, a logical experimental approach would be the use of FGF-23 blocking antibodies as the most direct strategy to inhibit FGF-23 actions in the uraemic context. Yet, in a preclinical model of CKD, rats treated with a neutralizing FGF-23 antibody presented elevated systemic serum phosphate and developed severe cardiovascular complications (Shalhoub et al., 2012). Thus, the key point would be not to fully suppress FGF-23 actions, such as the physiological phosphaturic action, but only to block its damaging actions on the heart. The second application would involve exogenous klotho administration as a therapeutic option to block the deleterious FGF-23 actions on the heart. Klotho is emerging as a potential cardioprotective factor for uraemic cardiomyopathy. Indeed, klotho protects against vascular calcification in human (Lim et al., 2012) and experimental models (Hu et al., 2011) of CKD. Moreover, sKL deficiency in CKD seems to render the myocardium more susceptible to stress-induced injury (Xie, Cha, An, Kuro-O, Birnbaumer & Huang, 2012). Similarly, some authors have proposed that FGF-23 induces cardiac toxicity only when serum levels of sKL are reduced in CKD (Hu et al., 2015), whereas other authors posit that klotho prevents uraemic cardiomyopathy by a direct effect on cardiomyocytes independently of FGF-23 and phosphates (Xie, Yoon, An, Kuro-o & Huang, 2015). Nevertheless, clinical studies on the predictive value of klotho have produced conflicting results, with some reporting that plasma sKL levels did not predict cardiovascular

events or death in a large CKD cohort (Seiler et al., 2013), while others demonstrated a clear association between preserved sKL levels and reduced cardiovascular morbidity and mortality in dialysis-dependent CKD (Hu et al., 2011). The idea that sKL could function as a decoy of FGF-23 actions in the heart is in agreement with our results. Thus, we observed a cardioprotective effect of rKL administration on preventing contractile dysfunction and diastolic Ca^{2+} leak related to pro-arrhythmic events in cardiomyocytes from Nfx mice. In this respect, klotho has been shown to produce beneficial cardiac actions on ionic channels, including the downregulation of transient receptor potential cation channel 6 (TRPC6) in conditions of cardiac hypertrophy (Xie, Cha, An, Kuro-O, Birnbaumer & Huang, 2012; Xie, Yoon, An, Kuro-o & Huang, 2015). However, in physiological conditions, the contribution of TRPC6 channels to the total Ca^{2+} entry in cardiomyocytes is small and is higher in conditions of cardiac hypertrophy. In the present study, we found no evidence of cardiac morphology changes such as hypertrophy or fibrosis in klotho hypomorphic mice and mice after 6 weeks of 5/6 nephrectomy. *Kl/kl* mice showed an increase in HW/BW ratio that was not accompanied by an increase in cardiomyocyte area, or ANP and collagen expression as specific markers of cellular hypertrophy or fibrosis, respectively. A possible explanation for these results is that klotho hypomorphic mice showed reduced BW compared to +/+ mice; and they also present an important growth retardation affecting all organs, which could explain the reduced cardiomyocyte areas or collagen levels compared to their +/+ littermates. Besides the absence of klotho expression also induces important ectopic calcification in arterial walls and cardiac muscle (Kuro-o et al., 1997; Yoshida, Fujimori & Nabeshima, 2002). All these facts might favour a higher HW/BW ratio than that expected for its body weight and animal size. Therefore, these results support the conclusion that Ca^{2+} mishandling observed in kl/kl mice is not due to cardiomyocyte hypertrophy or deleterious remodelling development, though the influence of systemic calcaemia and alterations in vitamin D homeostasis in this klotho mutant mice (Yoshida, Fujimori & Nabeshima, 2002) could not be discarded; specially on the elevated diastolic Ca^{2+} release and pro-arrhythmic events of kl/kl cardiomyocytes.

There is a general statement that the experimental CKD model shows a compromised EF and cardiac dysfunction in mice (Bro, Bollano, Brüel, Olgaard & Nielsen, 2008; Chen et al., 2017). However, there are apparently opposite results related to hypertrophy development that might appear together with this cardiac dysfunction. Thus, some authors have described Nfx-induced cardiac dysfunction with a significant increment of the heart weight (Chen et al., 2017) while other authors using the same experimental CKD model did not observe any increase in the

heart weight (Bro, Bollano, Brüel, Olgaard & Nielsen, 2008) as we have also observed in the present study. These apparently opposite results could be explained by the age of the animals used and also the time employed from 5/6 Nfx surgery to the cardiac analysis. In our hands, this experimental model of CKD developed a dysfunctional cardiac phenotype without hypertrophy or fibrosis development. This is an ideal *in vivo* model to study functional cardiac events such as heart failure and the predisposition to arrhythmia related to Ca^{2+} mishandling in the context of uraemic cardiomyopathy without any overlap due to structural myocardial alterations. Using this model, we demonstrate a cardioprotective role of klotho through the normalisation of cardiomyocyte Ca^{2+} cycling. Mechanistically, we propose that RyRs are a novel target of klotho, and klotho could act as a "brake" for the pro-arrhythmogenic Ca^{2+} leak from the SR by impeding phosphorylation and hyperactivation of RyRs previously observed in CKD. By halting Ca^{2+} leakage, klotho helps to maintain an adequate cellular shortening due to the recovery of systolic Ca^{2+} release in the form of Ca^{2+} transients and, at the same time, impedes the increase in diastolic Ca^{2+} release in the form of Ca^{2+} sparks or waves that might favour reaching a intracellular Ca^{2+} threshold able to evoke automatic Ca^{2+} transients and extracontractions. Finally, one of the most relevant findings of our study is that we show for the first time that klotho can protect the heart from Ca^{2+} mishandling associated with CKD without any associated improvement in renal dysfunction. Thus, Nfx mice overexpressing klotho or chronically treated with rKL present the same high systemic levels of FGF-23 and BUN as those Nfx mice treated with vehicle. We believe these findings are clinically relevant because strategies directed to maintain adequate klotho levels could be a new therapeutic goal to directly protect the heart from a uraemic environment and guaranteeing FGF-23 phosphaturic action.

One limitation of the present study is the lack of data in larger animal models that exhibit closer physiological characteristics to humans, such as rabbits or pigs. Moreover, further investigation will be required to determine in-depth whther the klotho deficiency, a very common aspect in CKD patients, might influence diastolic Ca^{2+} levels and therefore compromise cardiac contractility. We envision the need to corroborate the cardioprotective role of klotho throughout the development of renal disease from initial stages including in larger animal models in future studies.

Conclusion

This study provides new insights into how klotho availability determines cardiac function in uraemic cardiomyopathy via regulation of Ca^{2+} handling. The present investigation revealed

the dysregulated cardiac physiological mechanisms in uraemia modelled by klotho deficiency or nephrectomy, including defects in systolic Ca^{2+} release and contractile dysfunction together with RyR hyperactivation, which can explain the elevated presence of pro-arrhythmogenic Ca^{2+} events found in a uraemic setting. All of these alterations in Ca^{2+} handling observed in CKD mice were prevented when klotho was present, indicating that therapeutic strategies directed to improve klotho availability might be good candidates to protect the heart from cardiac dysfunction and arrhythmogenic potential events in CKD.

Declaration of transparency and scientific rigour

This Declaration acknowledges that this paper adheres to the principles for transparent reporting and scientific rigour of preclinical research as stated in the *BJP* guidelines for Natural Product Research, Design and Analysis, Immunoblotting and Immunochemistry, and Animal Experimentation, and as recommended by funding agencies, publishers and other organisations engaged with supporting research.

References:

Alexander SPH, Roberts RE, Broughton BRS, Sobey CG, George CH, Stanford SC, *et al.* (2018). Goals and practicalities of immunoblotting and immunohistochemistry: A guide for submission to the British Journal of Pharmacology. Br J Pharmacol 175**:** 407-411.

Asai O, Nakatani K, Tanaka T, Sakan H, Imura A, Yoshimoto S, *et al.* (2012). Decreased renal α-Klotho expression in early diabetic nephropathy in humans and mice and its possible role in urinary calcium excretion. Kidney Int 81**:** 539-547.

Banerjee D (2016). Sudden cardiac death in haemodialysis: clinical epidemiology and mechanisms. J Electrocardiol 49**:** 843-847.

Bell JR, Raaijmakers AJ, Curl CL, Reichelt ME, Harding TW, Bei A, *et al.* (2015). Cardiac CaMKIIδ splice variants exhibit target signaling specificity and confer sex-selective arrhythmogenic actions in the ischemic-reperfused heart. Int J Cardiol 181**:** 288-296.

Bergmark BA, Udell JA, Morrow DA, Jarolim P, Kuder JF, Solomon SD, *et al.* (2019). Klotho, fibroblast growth factor-23, and the renin-angiotensin system - an analysis from the PEACE trial. Eur J Heart Fail 21**:** 462-470.

Bers DM (2002). Cardiac excitation-contraction coupling. Nature 415**:** 198-205.

Bers DM (2014). Cardiac sarcoplasmic reticulum calcium leak: basis and roles in cardiac dysfunction. Annu Rev Physiol 76**:** 107-127.

Bode EF, Briston SJ, Overend CL, O'Neill SC, Trafford AW, & Eisner DA (2011). Changes of SERCA activity have only modest effects on sarcoplasmic reticulum Ca2+ content in rat ventricular myocytes. J Physiol 589**:** 4723-4729.

Bro S, Bollano E, Brüel A, Olgaard K, & Nielsen LB (2008). Cardiac structure and function in a mouse model of uraemia without hypertension. Scand J Clin Lab Invest 68**:** 660-666.

Charytan DM, Foley R, McCullough PA, Rogers JD, Zimetbaum P, Herzog CA, *et al.* (2016). Arrhythmia and Sudden Death in Hemodialysis Patients: Protocol and Baseline Characteristics of the Monitoring in Dialysis Study. Clin J Am Soc Nephrol 11**:** 721-734.

Chen J, Kieswich JE, Chiazza F, Moyes AJ, Gobbetti T, Purvis GS, *et al.* (2017). IκB Kinase Inhibitor Attenuates Sepsis-Induced Cardiac Dysfunction in CKD. J Am Soc Nephrol 28**:** 94-105.

Cheng H, Song LS, Shirokova N, González A, Lakatta EG, Ríos E, *et al.* (1999). Amplitude distribution of calcium sparks in confocal images: theory and studies with an automatic detection method. Biophys J 76**:** 606-617.

Coll M, Ferrer-Costa C, Pich S, Allegue C, Rodrigo E, Fernández-Fresnedo G, *et al.* (2018). Role of genetic and electrolyte abnormalities in prolonged QTc interval and sudden cardiac death in end-stage renal disease patients. PLoS One 13**:** e0200756.

Coresh J, Selvin E, Stevens LA, Manzi J, Kusek JW, Eggers P, *et al.* (2007). Prevalence of chronic kidney disease in the United States. JAMA 298**:** 2038-2047.

Curtis MJ, Bond RA, Spina D, Ahluwalia A, Alexander SP, Giembycz MA, *et al.* (2015). Experimental design and analysis and their reporting: new guidance for publication in BJP. Br J Pharmacol 172**:** 3461-3471.

de Alba-Aguayo DR, Pavón N, Mercado-Morales M, Miranda-Saturnino M, López-Casamichana M, Guerrero-Hernández A, *et al.* (2017). Increased calcium leak associated with reduced calsequestrin expression in hyperthyroid cardiomyocytes. Cell Calcium 62**:** 29-40.

Delgado C, Gomez AM, Samia El Hayek M, Ruiz-Hurtado G, & Pereira L (2019). Gender-Dependent Alteration of Ca. Front Physiol 10**:** 40.

Dhindwal S, Lobo J, Cabra V, Santiago DJ, Nayak AR, Dryden K, *et al.* (2017). A cryo-EM-based model of phosphorylation- and FKBP12.6-mediated allosterism of the cardiac ryanodine receptor. Sci Signal 10 (480).

Faul C (2018). FGF23 effects on the heart-levels, time, source, and context matter. Kidney Int 94**:** 7-11.

Fernández-Velasco M, Rueda A, Rizzi N, Benitah JP, Colombi B, Napolitano C, *et al.* (2009). Increased Ca2+ sensitivity of the ryanodine receptor mutant RyR2R4496C underlies catecholaminergic polymorphic ventricular tachycardia. Circ Res 104**:** 201-209, 212p following 209.

Gagnon RF, & Gallimore B (1988). Characterization of a mouse model of chronic uremia. Urol Res 16**:** 119-126.

Go AS, Chertow GM, Fan D, McCulloch CE, & Hsu CY (2004). Chronic kidney disease and the risks of death, cardiovascular events, and hospitalization. N Engl J Med 351**:** 1296-1305.

Grimm M, Ling H, Willeford A, Pereira L, Gray CB, Erickson JR, *et al.* (2015). CaMKIIδ mediates β-adrenergic effects on RyR2 phosphorylation and SR Ca(2+) leak and the pathophysiological response to chronic β-adrenergic stimulation. J Mol Cell Cardiol 85**:** 282-291.

Gutiérrez OM, Mannstadt M, Isakova T, Rauh-Hain JA, Tamez H, Shah A, *et al.* (2008). Fibroblast growth factor 23 and mortality among patients undergoing hemodialysis. N Engl J Med 359**:** 584-592.

Herzog CA, Asinger RW, Berger AK, Charytan DM, Díez J, Hart RG, *et al.* (2011). Cardiovascular disease in chronic kidney disease. A clinical update from Kidney Disease: Improving Global Outcomes (KDIGO). Kidney Int 80**:** 572-586.

Heveran CM, Schurman CA, Acevedo C, Livingston EW, Howe D, Schaible EG, *et al.* (2019). Chronic kidney disease and aging differentially diminish bone material and microarchitecture in C57Bl/6 mice. Bone 127**:** 91-103.

Hu MC, Shi M, Cho HJ, Adams-Huet B, Paek J, Hill K, *et al.* (2015). Klotho and phosphate are modulators of pathologic uremic cardiac remodeling. J Am Soc Nephrol 26**:** 1290-1302.

Hu MC, Shi M, Gillings N, Flores B, Takahashi M, Kuro-O M, *et al.* (2017). Recombinant α-Klotho may be prophylactic and therapeutic for acute to chronic kidney disease progression and uremic cardiomyopathy. Kidney Int 91**:** 1104-1114.

Hu MC, Shi M, Zhang J, Quiñones H, Griffith C, Kuro-o M, *et al.* (2011). Klotho deficiency causes vascular calcification in chronic kidney disease. J Am Soc Nephrol 22**:** 124-136.

Isakova T, Cai X, Lee J, Xie D, Wang X, Mehta R, *et al.* (2018). Longitudinal FGF23 Trajectories and Mortality in Patients with CKD. J Am Soc Nephrol 29**:** 579-590.

Isakova T, Xie H, Yang W, Xie D, Anderson AH, Scialla J, *et al.* (2011). Fibroblast growth factor 23 and risks of mortality and end-stage renal disease in patients with chronic kidney disease. JAMA 305**:** 2432-2439.

Kao YH, Chen YC, Lin YK, Shiu RJ, Chao TF, Chen SA, *et al.* (2014). FGF-23 dysregulates calcium homeostasis and electrophysiological properties in HL-1 atrial cells. Eur J Clin Invest 44**:** 795-801.

Kilkenny C, Browne WJ, Cuthill IC, Emerson M, & Altman DG (2010). Improving bioscience research reporting: The ARRIVE guidelines for reporting animal research. J Pharmacol Pharmacother 1**:** 94-99.

Kuro-o M (2011). Klotho and the aging process. Korean J Intern Med 26**:** 113-122.

Kuro-O M (2011). Phosphate and Klotho. Kidney Int 79121**:** S20-23.

Kuro-o M, Matsumura Y, Aizawa H, Kawaguchi H, Suga T, Utsugi T, *et al.* (1997). Mutation of the mouse klotho gene leads to a syndrome resembling ageing. Nature 390**:** 45-51.

Lim K, Lu TS, Molostvov G, Lee C, Lam FT, Zehnder D, *et al.* (2012). Vascular Klotho deficiency potentiates the development of human artery calcification and mediates resistance to fibroblast growth factor 23. Circulation 125**:** 2243-2255.

McGrath JC, Drummond GB, McLachlan EM, Kilkenny C, & Wainwright CL (2010). Guidelines for reporting experiments involving animals: the ARRIVE guidelines. Br J Pharmacol 160**:** 1573-1576.

Memmos E, Sarafidis P, Pateinakis P, Tsiantoulas A, Faitatzidou D, Giamalis P, *et al.* (2019). Soluble Klotho is associated with mortality and cardiovascular events in hemodialysis. BMC Nephrol 20**:** 217.

Nattel S, Maguy A, Le Bouter S, & Yeh YH (2007). Arrhythmogenic ion-channel remodeling in the heart: heart failure, myocardial infarction, and atrial fibrillation. Physiol Rev 87**:** 425-456.

Navarro-García JA, Delgado C, Fernández-Velasco M, Val-Blasco A, Rodríguez-Sánchez E, Aceves-Ripoll J, *et al.* (2019). Fibroblast growth factor-23 promotes rhythm alterations and contractile dysfunction in adult ventricular cardiomyocytes. Nephrol Dial Transplant 34(11):1864-1875.

Nowak A, Friedrich B, Artunc F, Serra AL, Breidthardt T, Twerenbold R, *et al.* (2014). Prognostic value and link to atrial fibrillation of soluble Klotho and FGF23 in hemodialysis patients. PLoS One 9(7)**:** e100688.

Parks RJ, Ray G, Bienvenu LA, Rose RA, & Howlett SE (2014). Sex differences in SR Ca(2+) release in murine ventricular myocytes are regulated by the cAMP/PKA pathway. J Mol Cell Cardiol 75**:** 162-173.

Pavik I, Jaeger P, Ebner L, Wagner CA, Petzold K, Spichtig D, *et al.* (2013). Secreted Klotho and FGF23 in chronic kidney disease Stage 1 to 5: a sequence suggested from a cross-sectional study. Nephrol Dial Transplant 28**:** 352-359.

Pereira L, Ruiz-Hurtado G, Rueda A, Mercadier JJ, Benitah JP, & Gómez AM (2014). Calcium signaling in diabetic cardiomyocytes. Cell Calcium 56**:** 372-380.

Ruiz-Hurtado G, Li L, Fernández-Velasco M, Rueda A, Lefebvre F, Wang Y, *et al.* (2015). Reconciling depressed Ca2+ sparks occurrence with enhanced RyR2 activity in failing mice cardiomyocytes. J Gen Physiol 146**:** 295-306.

Seiler S, Wen M, Roth HJ, Fehrenz M, Flügge F, Herath E, *et al.* (2013). Plasma Klotho is not related to kidney function and does not predict adverse outcome in patients with chronic kidney disease. Kidney Int 83**:** 121-128.

Semba RD, Cappola AR, Sun K, Bandinelli S, Dalal M, Crasto C, *et al.* (2011). Plasma klotho and cardiovascular disease in adults. J Am Geriatr Soc 59**:** 1596-1601.

Shalhoub V, Shatzen EM, Ward SC, Davis J, Stevens J, Bi V, *et al.* (2012). FGF23 neutralization improves chronic kidney disease-associated hyperparathyroidism yet increases mortality. J Clin Invest 122**:** 2543-2553.

Shioya T (2007). A simple technique for isolating healthy heart cells from mouse models. J Physiol Sci 57**:** 327-335.

Touchberry CD, Green TM, Tchikrizov V, Mannix JE, Mao TF, Carney BW, *et al.* (2013). FGF23 is a novel regulator of intracellular calcium and cardiac contractility in addition to cardiac hypertrophy. Am J Physiol Endocrinol Metab 304**:** E863-873.

Urakawa I, Yamazaki Y, Shimada T, Iijima K, Hasegawa H, Okawa K, *et al.* (2006). Klotho converts canonical FGF receptor into a specific receptor for FGF23. Nature 444**:** 770-774.

Verde E, Pérez de Prado A, López-Gómez JM, Quiroga B, Goicoechea M, García-Prieto A, *et al.* (2016). Asymptomatic Intradialytic Supraventricular Arrhythmias and Adverse Outcomes in Patients on Hemodialysis. Clin J Am Soc Nephrol 11**:** 2210-2217.

Wanner C, Amann K, & Shoji T (2016). The heart and vascular system in dialysis. Lancet 388**:** 276-284.

Xiao B, Jiang MT, Zhao M, Yang D, Sutherland C, Lai FA, *et al.* (2005). Characterization of a novel PKA phosphorylation site, serine-2030, reveals no PKA hyperphosphorylation of the cardiac ryanodine receptor in canine heart failure. Circ Res 96**:** 847-855.

Xie J, Cha SK, An SW, Kuro-O M, Birnbaumer L, & Huang CL (2012). Cardioprotection by Klotho through downregulation of TRPC6 channels in the mouse heart. Nat Commun 3**:** 1238.

Xie J, Yoon J, An SW, Kuro-o M, & Huang CL (2015). Soluble Klotho Protects against Uremic Cardiomyopathy Independently of Fibroblast Growth Factor 23 and Phosphate. J Am Soc Nephrol 26**:** 1150-1160.

Yoshida T, Fujimori T, & Nabeshima Y (2002). Mediation of unusually high concentrations of 1,25-dihydroxyvitamin D in homozygous klotho mutant mice by increased expression of renal 1alpha-hydroxylase gene. Endocrinology 143**:** 683-689.

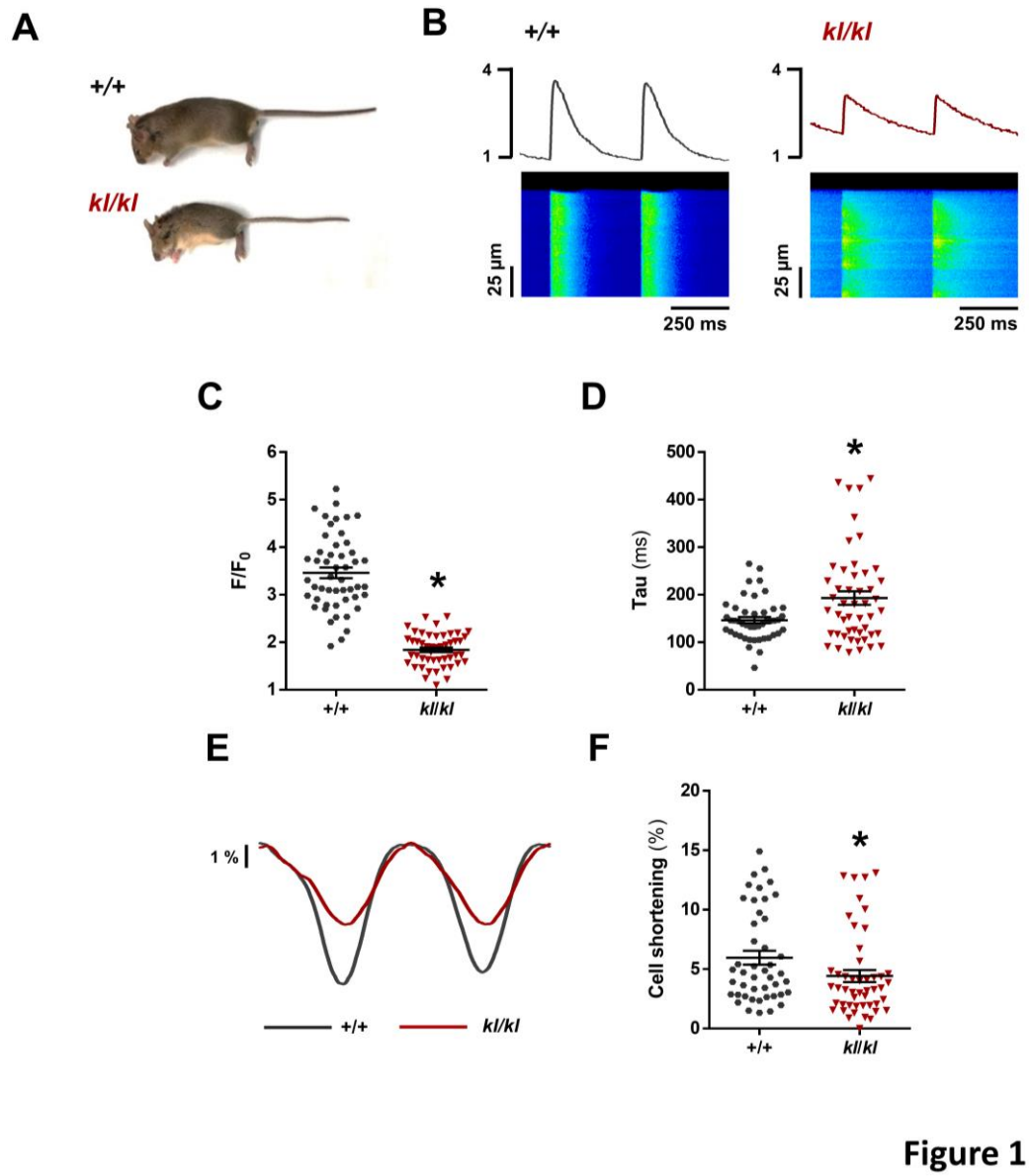

Figure 1

Figure 1. Klotho deficiency impairs systolic Ca^{2+} release and induces contractile dysfunction. (A) Appearance of 7-week-old wild-type (+/+) mouse and its Klotho-hypomorphic (*kl/kl*) littermate. **(B)** Line-scan images and fluorescence profiles of cardiomyocytes under 2 Hz field stimulation. **(C&D)** Mean values of peak (F/F_0) (C) and time of decay (*Tau*) (D) of electrically-evoked Ca^{2+} transients in +/+ (n=50 cells/N=5 mice) and *kl/kl* (n=49 cells/N=5 mice). **(E)** Cell shortening profiles of cardiomyocytes. **(F)** Percentage of cell contraction of +/+ (n=50 cells/N=5 mice) and *kl/kl* (n=49 cells/N=5 mice). Data are shown as mean±SEM. $^{*}P<0.05$ vs. +/+.

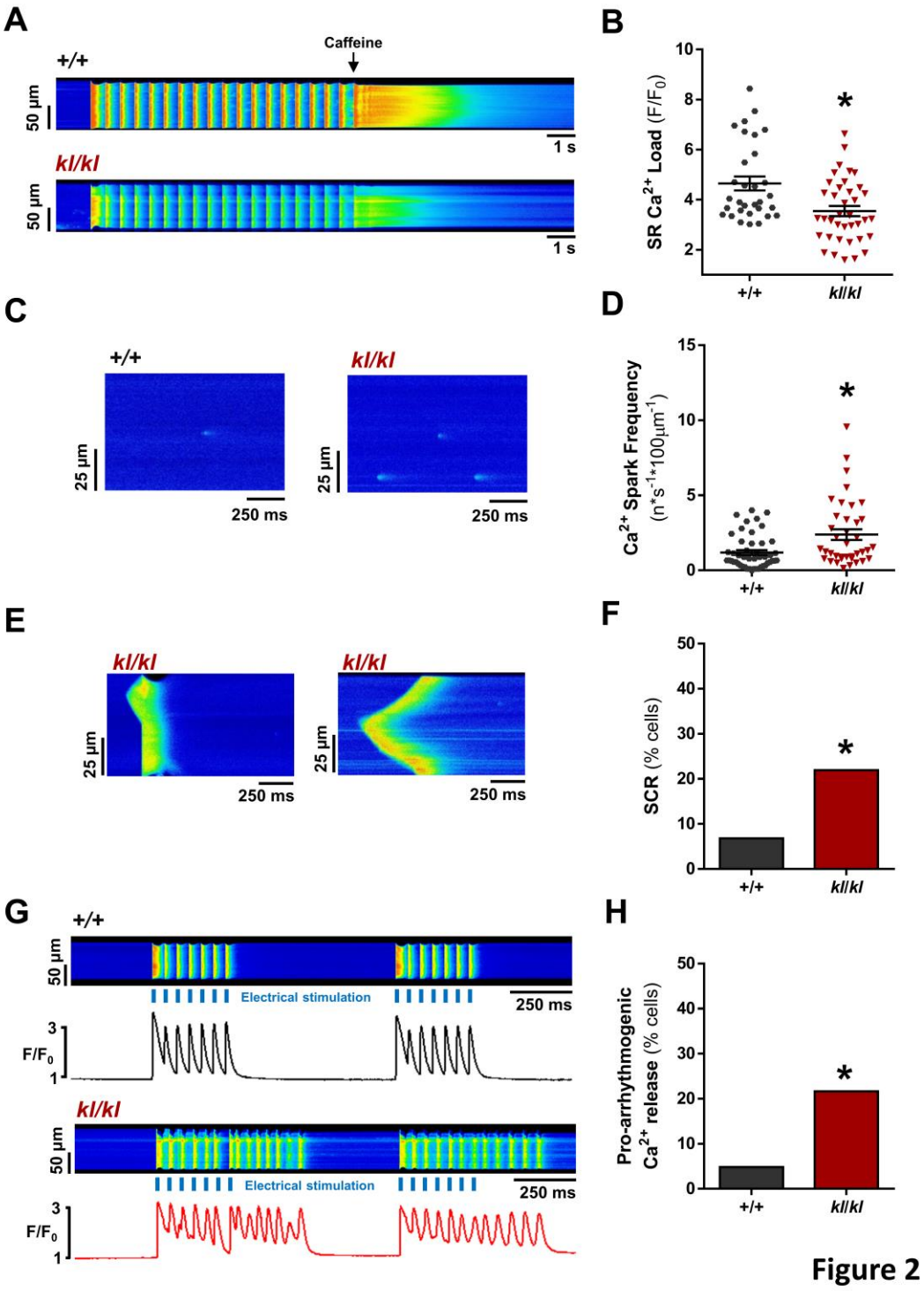

Figure 2

Figure 2. Klotho deficiency reduces SR-Ca^{2+} load and increases diastolic Ca^{2+} leak and pro-arrhythmogenic events. (A) Line-scan images of cardiomyocytes under 2 Hz field stimulation perfused with caffeine. **(B)** Mean values of caffeine-evoked Ca^{2+} transients amplitude expressed as peak (F/F_0) in +/+ (n=31 cells/N=5 mice) and *kl/kl* (n=39 cells/N=5 mice). **(C)** Line-scan images of spark recordings in quiescent cardiomyocytes. **(D)** Mean values

of Ca^{2+} spark frequency in +/+ (664 sparks, n=48 cells/N=5 mice) and *kl/kl* (630 sparks, n=39 cells/N=5 mice). **(E)** Line-scan images of spontaneous Ca^{2+} release (SCR) as spontaneous Ca^{2+} transients (left panel) or Ca^{2+} waves (right panel) in quiescent *kl/kl* cardiomyocytes. **(F)** Occurrence of SCR in +/+ (n=48 cells/N=5 mice) and *kl/kl* (n=39 cells/N=5 mice). **(G)** Line-scan images and fluorescence profiles of cardiomyocytes paced at 2 Hz field stimulation. **(H)** Occurrence of pro-arrhythmogenic events related to automatic Ca^{2+} transients and automatic contractions in +/+ (n=26 cells/ N= 5 mice) and *kl/kl* (n=38 cells/N=5 mice) mice. Data are shown as mean±SEM. $^{*}P<0.05$ vs. +/+.

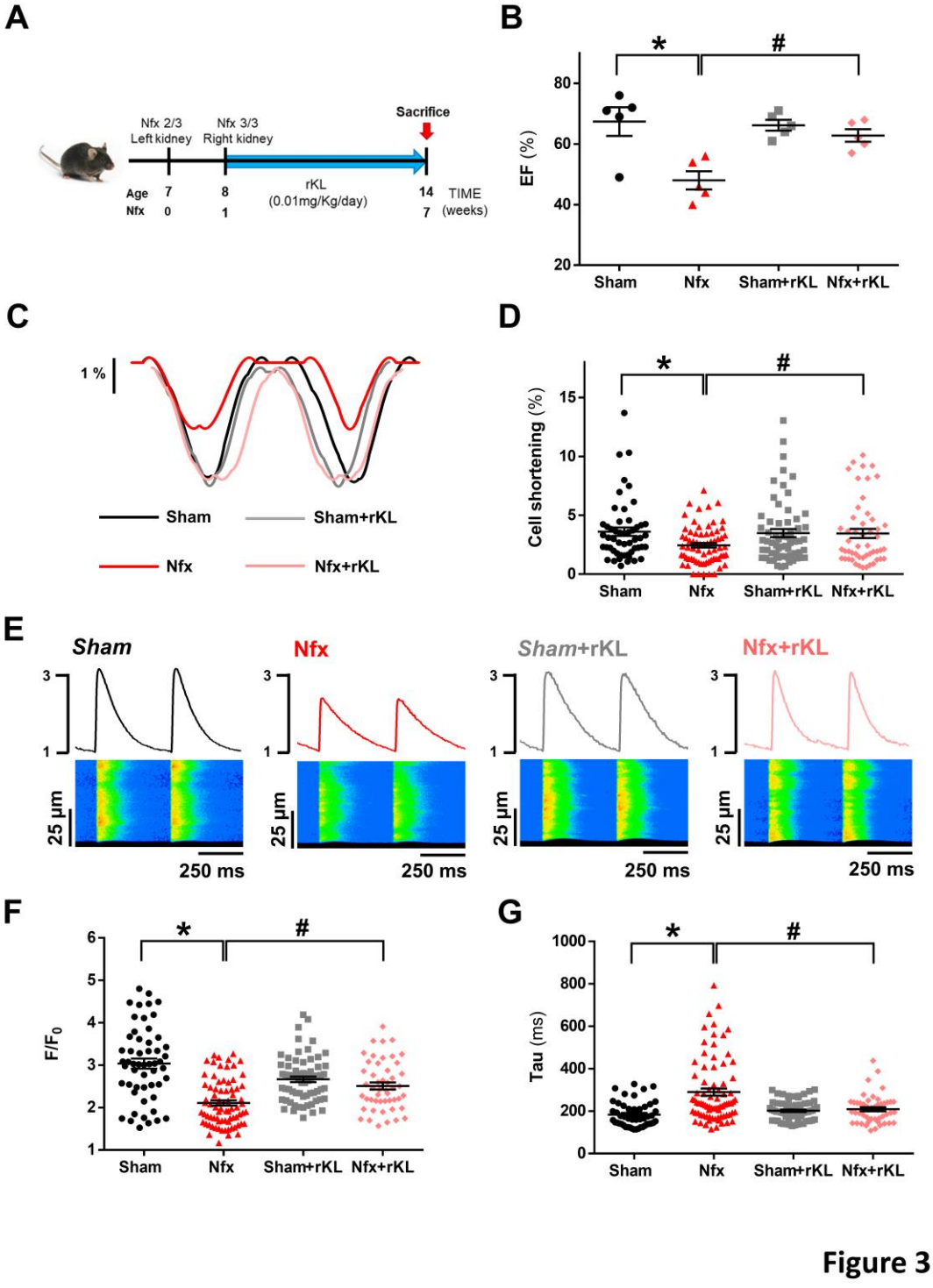

Figure 3

Figure 3. Recombinant klotho prevents contractile cellular dysfunction and reduction in systolic Ca^{2+}. (A) Schematic design of CKD animal model (5/6 nephrectomy) and treatments. **(B)** Mean values of ejection fraction (EF) from *Sham* (N=5 mice), Nfx (N=5 mice), *Sham*+rKL (N=5 mice) and Nfx+rKL (N=5 mice) mouse hearts. **(C)** Cell shortening profiles of cardiomyocytes. **(D)** Percentage of cell contraction of *Sham* (n=52 cells/N=5 mice), Nfx (n=73 cells/N=6 mice), *Sham*+rKL (n=62 cells/N=5 mice) and Nfx+rKL (n=48 cells/N=6 mice). **(E)**

Line-scan images and fluorescence profiles of cardiomyocytes under 2 Hz field stimulation. **(F&G)** Mean values of peak (F/F_0) (F) and time of decay (*Tau*) (G) of electrically-evoked Ca^{2+} transients in *Sham* (n=54 cells/N=5 mice), Nfx (n=77 cells/N=6 mice), *Sham*+rKL (n=67 cells/N=5 mice) and Nfx+rKL (n=49 cells/N=6 mice). Data shown mean±SEM. $^{*}P<0.05$ vs. *Sham* and $^{\#}P<0.05$ vs. Nfx.

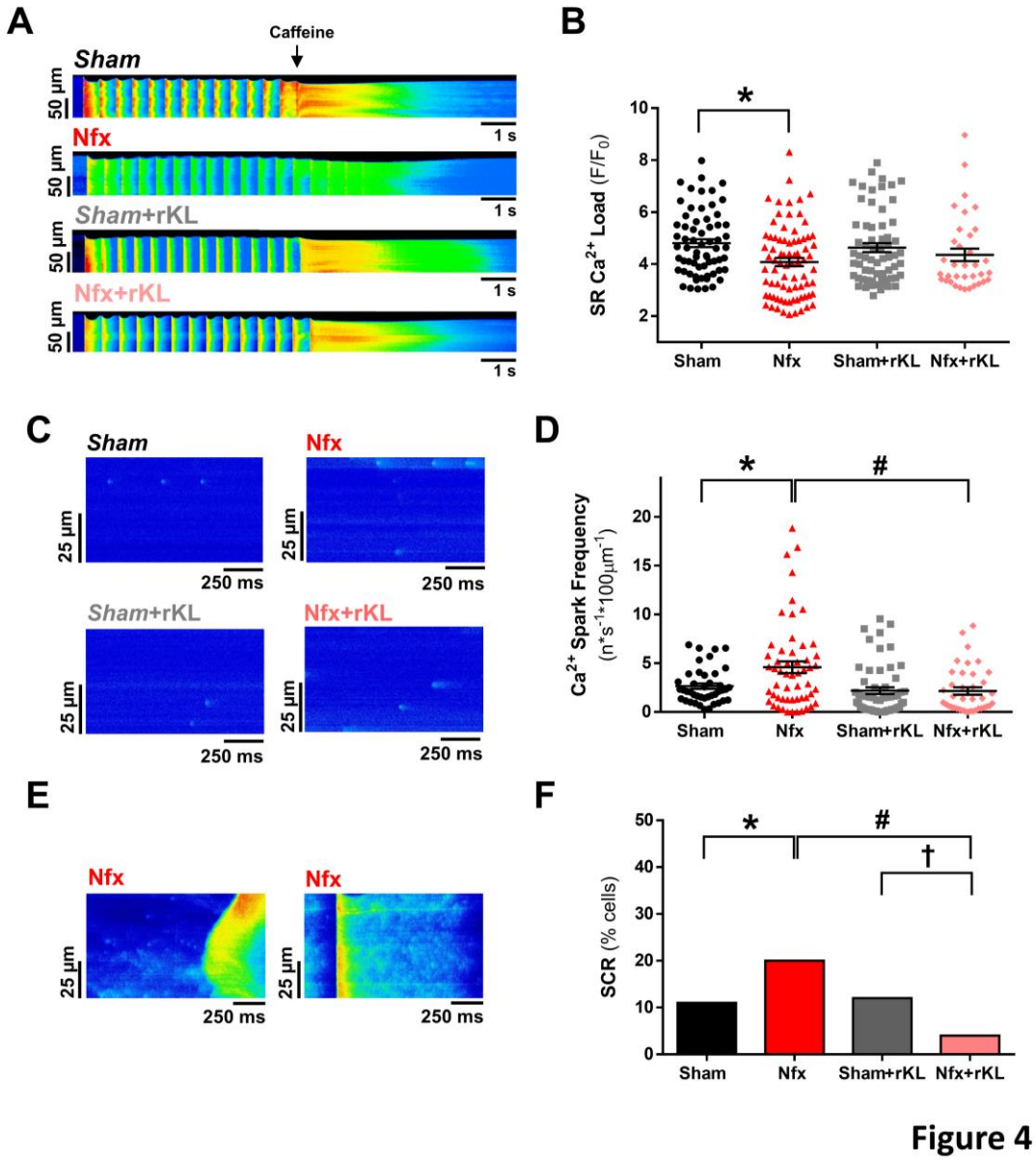

Figure 4

Figure 4. Recombinant klotho prevents SR-Ca^{2+} load and diastolic SR-Ca^{2+} leak in experimental CKD. (A) Line-scan images of cardiomyocytes under 2 Hz field stimulation perfused with caffeine. **(B)** Mean values of caffeine-evoked Ca^{2+} transients amplitude expressed as peak (F/F_0) in *Sham* (n=66 cells/N=6 mice), Nfx (n=79 cells/N=6 mice), *Sham*+rKL (n=67 cells/N=6 mice) and Nfx+rKL (n=49 cells/N=6 mice) cardiomyoyctes. **(C)** Line-scan images of spark recordings in quiescent cardiomyocytes. **(D)** Mean values of Ca^{2+} spark frequency in *Sham* (1270 sparks, n=42 cells/N=5 mice), Nfx (2985 sparks, n=55 cells/N=6 mice), *Sham*+rKL (1188 sparks, n=56 cells/N=5 mice) and Nfx+rKL (1075 sparks, n=39 cells/N=6 mice). **(E)** Line-scan images of spontaneous Ca^{2+} release (SCR) as Ca^{2+} waves

(left panel) or spontaneous Ca^{2+} transients (right panel) in quiescent Nfx cardiomyocytes. **(F)** Occurrence of SCR in *Sham* (n=42 cells/N=5 mice), Nfx (n=55 cells/N=6 mice), *Sham*+rKL (n=56 cells/N=5 mice) and Nfx+rKL (n=39 cells/N=6 mice) cardiomyocytes. Data are shown as mean±SEM. $^{*}P<0.05$ vs. *Sham*; $^{\#}P<0.05$ vs. Nfx; and $^{\dagger}P<0.05$ vs *Sham*+rKL.

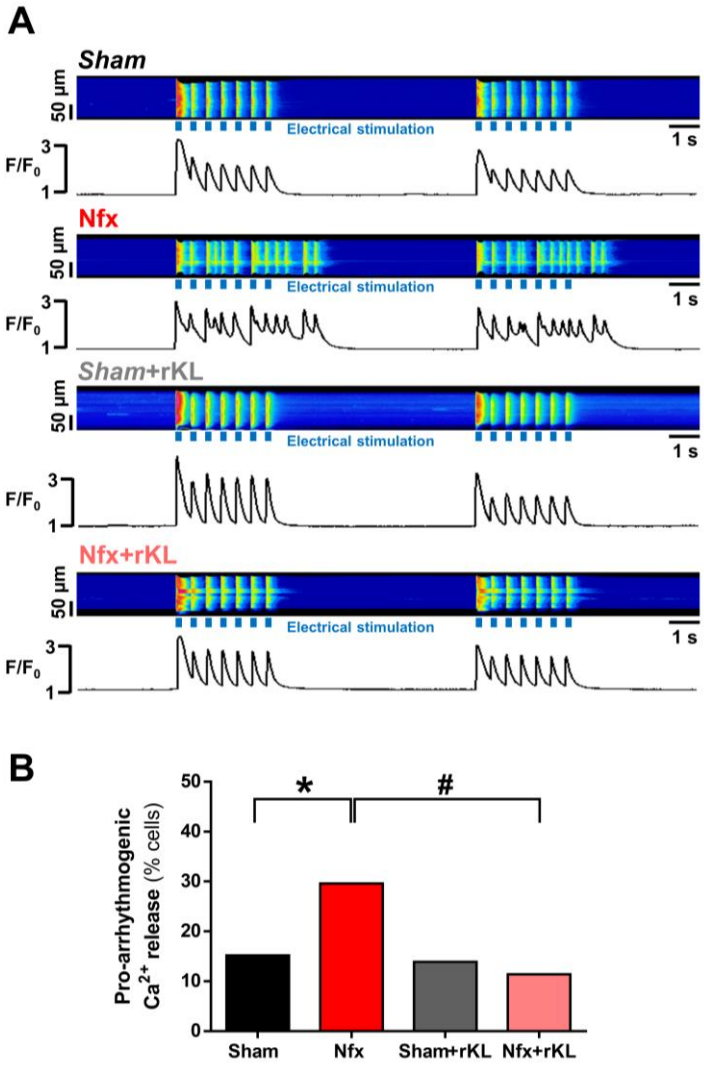

Figure 5

Figure 5. Recombinant klotho treatment impedes pro-arrhythmogenic events induced by Nfx. (A) Line-scan images and fluorescence profiles of cardiomyocytes paced at 2 Hz field stimulation. **(B)** Occurrence of pro-arrhythmogenic events related to automatic $Ca^{2+}{}_I$ transients and automatic contractions in *Sham* (n=92 cells/N= 5 mice), Nfx (n=142 cells/N=6 mice), *Sham*+rKL (n=72 cells/N=5 mice) and Nfx+rKL (n=149 cells/N=7 mice) mice. Data are shown as mean±SEM. $^{*}P<0.05$ vs. *Sham* and $^{\#}P<0.05$ vs. Nfx.

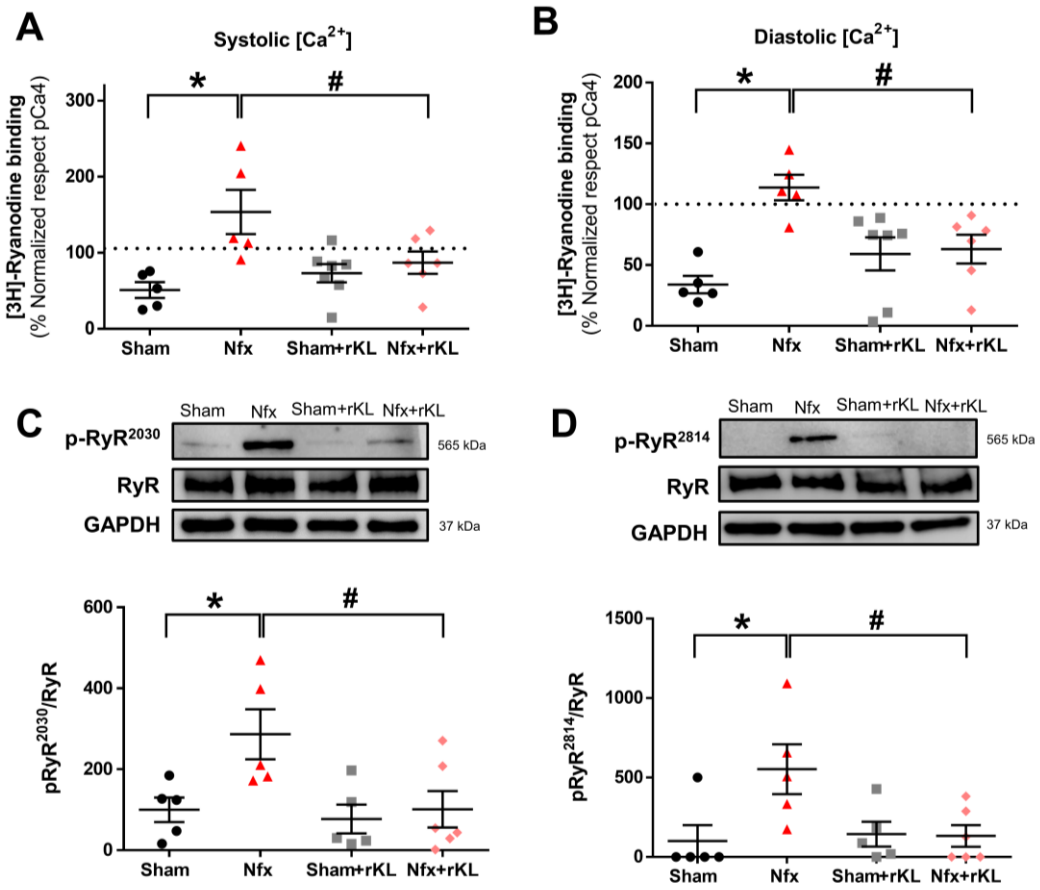

Figure 6

Figure 6. Recombinant klotho protects against RyR hyperactivation in experimental CKD. (A-B) Specific [^{3}H]-Ryanodine binding at (A) 10 µM (equivalent to the intracellular Ca^{2+} rise in systole) and (B) 100 nM (equivalent to basal levels of intracellular Ca^{2+} in quiescent conditions or diastole) and free Ca^{2+} concentrations of heart homogenates from *Sham* (N=5 mice), Nfx (N=5 mice), *Sham*+rKL (N=7 mice) and Nfx+rKL (N=6 mice). [^{3}H]-Ryanodine binding values were normalised to the specific [^{3}H]-Ryanodine binding at 100 µM free [Ca^{2+}]. **(C-D)** Western blots (upper panels) and quantification (bottom panels) of RyR phosphorylation at Ser^{2030} (p-RyR^{2030}) or at Ser^{2814} (p-RyR^{2814}) normalised to total RyR from *Sham* (N=5 mice), Nfx (N=7 mice), *Sham*+rKL (N=5 mice) and Nfx+rKL (N=7 mice) hearts. Data are shown as mean±SEM. $^{*}P<0.05$ vs. *Sham*; $^{\#}P<0.05$ vs. Nfx.

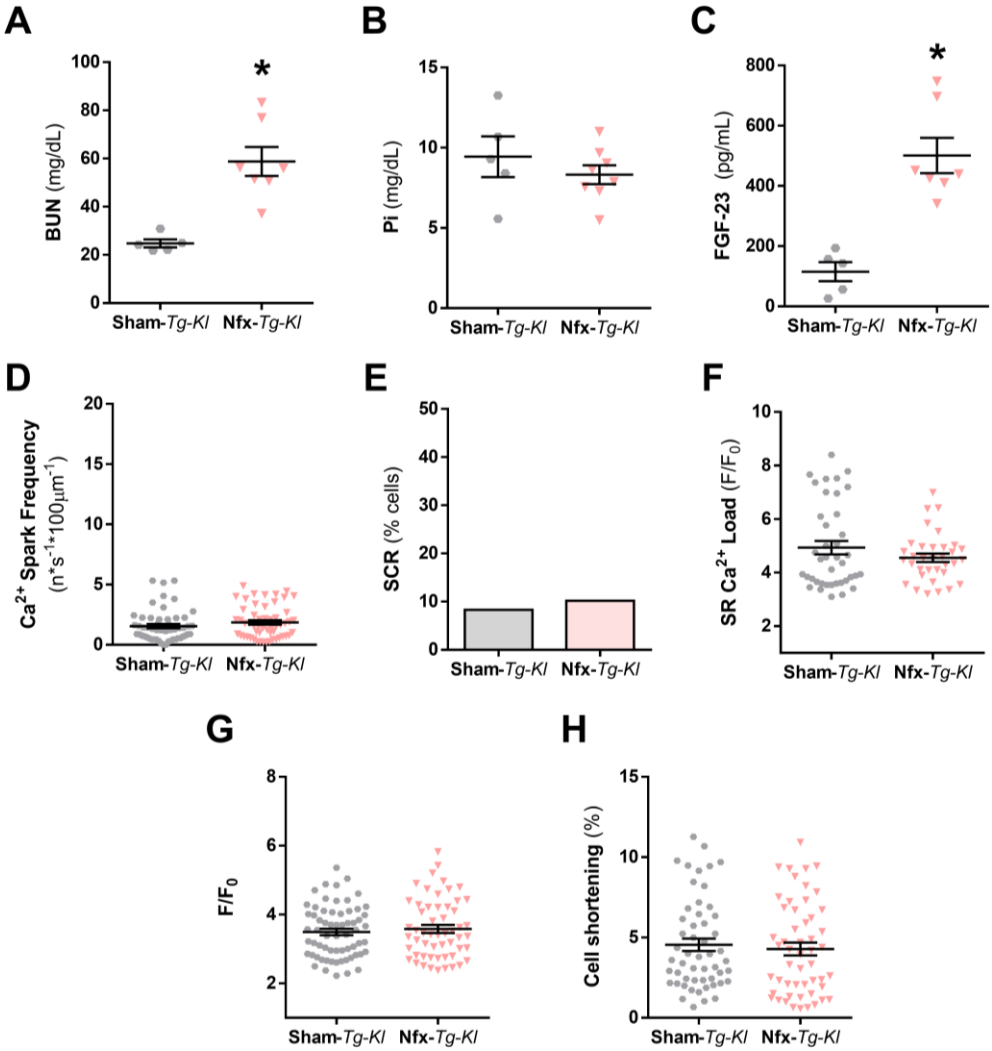

Figure 7

Figure 7. Klotho overexpression protects from electrical cardiac and Ca^{2+} cycling alterations induced by CKD. (A-C) Mean serum levels of (A) blood urea nitrogen (BUN), (B) phosphates (Pi) and (C) FGF-23 in *Sham-Tg-Kl* (N=5 mice) and Nfx-*Tg-Kl* (N=5 mice). **(D)** Mean values of Ca^{2+} sparks frequency in *Sham-Tg-Kl* (995 sparks, n=54 cells/N=5 mice), Nfx-*Tg-Kl* (893 sparks, n=55 cells/N=6 mice). **(E)** Occurrence of SCR in *Sham-Tg-Kl* (n=54 cells/N=5 mice), Nfx-*Tg-Kl* (n=55 cells/N=6 mice). **(F)** Mean values of caffeine-evoked Ca^{2+} transients amplitude expressed as peak (F/F_0) in *Sham-Tg-Kl* (n=40 cells/N=5 mice), Nfx-*Tg-Kl* (n=34 cells/N=6 mice). **(G)** Mean values of peak (F/F_0) of electrically-evoked Ca^{2+} transients in *Sham-Tg-Kl* (n=64 cells/N=5 mice), Nfx-*Tg-Kl* (n=55 cells/N=6 mice) **(H)** Percentage of cell contraction of *Sham-Tg-Kl* (n=56 cells/N=5 mice) and Nfx-*Tg-Kl* (n=52 cells/N=6 mice). Data are shown as mean±SEM. $^{*}P<0.05$ vs. *Sham-Tg-Kl*.